

**Remote Sensing and Geographic Information System
Approach for Hydrological, Morphometrical and Spatial
Analysis of Vishwamitri Watershed**

A Executive summary of the Ph.D thesis Submitted to
The Maharaja Sayajirao University of Baroda
in Fulfilment of the Requirements for the Award of Degree of

**DOCTOR OF PHILOSOPHY
IN
CIVIL ENGINEERING**

GUIDE

Dr. T.M.V SURYANARAYANA
Director, WREMI
Ph.D. in CIVIL ENGINEERING
Fellow- I.W.R.S.
Fellow- I.S.H.
M.I.A.H.S., M.A.H.I., M.A.P.H.W.,
M.I.S.G., M.A.A.M.

SUBMITTED BY

VIKAS KUMAR RANA
M.E (CIVIL) in WRE

**WATER RESOURCES ENGINEERING AND MANAGEMENT INSTITUTE
FACULTY OF TECHNOLOGY & ENGINEERING
THE MAHARAJA SAYAJIRAO UNIVERSITY OF BARODA
SAMIALA-391410 DIST: VADODARA**

July 2021

Table of Contents of Thesis

1. Introduction.....	Error! Bookmark not defined.
2. Literature Review	Error! Bookmark not defined.
2.1. General.....	Error! Bookmark not defined.
2.2. Literature review:.....	Error! Bookmark not defined.
1. Objective: To demonstrate a comparative assessment of discrepancy in the hydrological behaviour of the DEMs in terms of terrain representation at the catchment scale.	Error! Bookmark not defined.
2. Objective: To develop an approach to analyze Sentinel–2 satellite data using traditional and principal component analysis based approaches to create land use and land cover map, which is a prerequisite for developing the curve number.	Error! Bookmark not defined.
3. Objective: To perform Morphometrical analysis of Vishwamitri watershed and prioritization of sub-watersheds for assessing the flood influencing characteristics of sub-watersheds of the Vishwamitri river.....	Error! Bookmark not defined.
4. Objective: To identify potential runoff storage zones based on the various physical characteristics of the Vishwamitri watershed using a GIS-based conceptual framework that combines through analytic hierarchy process using multi criteria decision-making method.....	Error! Bookmark not defined.
5. Objective: To develop an approach for operational flood extent mapping using Synthetic Aperture Radar (SAR) and preparation of flood inundation map for data scarce region using 2D flow modelling using rain on grid model.	Error! Bookmark not defined.
6. Objective: To quantify the effects of urban land forms on land surface temperature and modeling the spatial variation using machine learning.	Error! Bookmark not defined.
3. Study Area and Data Collection	Error! Bookmark not defined.
3.1 General.....	Error! Bookmark not defined.
3.2 Study areas and Data collection	Error! Bookmark not defined.
4. Methodology	Error! Bookmark not defined.
4.1 General.....	Error! Bookmark not defined.
4.2 Methodology	Error! Bookmark not defined.
1. Objective: To demonstrate a comparative assessment of discrepancy in the hydrological behaviour of the DEMs in terms of terrain representation at the catchment scale.	Error! Bookmark not defined.
2. Objective: To develop an approach to analyze Sentinel–2 satellite images using traditional and principal component analysis based approaches to create land use and land cover map, which is a prerequisite for developing the curve number.	Error! Bookmark not defined.
3. Objective: To perform Morphometrical analysis of Vishwamitri watershed and prioritization of sub-watersheds for assessing the flood influencing characteristics of sub-watersheds of the Vishwamitri river.....	Error! Bookmark not defined.

4. **Objective:** To identify potential runoff storage zones based on the various physical characteristics of the Vishwamitri watershed using a GIS-based conceptual framework that combines through analytic hierarchy process using multi criteria decision-making method..... **Error! Bookmark not defined.**
5. **Objective:** To develop an approach for operational flood extent mapping using Synthetic Aperture Radar (SAR) and preparation of flood inundation map for data scarce region using 2D flow modelling using rain on grid model. **Error! Bookmark not defined.**
6. **Objective:** To quantify the effects of urban land forms on land surface temperature and modeling the spatial variation using machine learning. **Error! Bookmark not defined.**
5. **Results and analysis** **Error! Bookmark not defined.**
 - 5.1 **General**..... **Error! Bookmark not defined.**
 - 5.2 **Results and analysis**..... **Error! Bookmark not defined.**
 1. **Objective:** To demonstrate a comparative assessment of discrepancy in the hydrological behaviour of the DEMs in terms of terrain representation at the catchment scale. **Error! Bookmark not defined.**
 2. **Objective:** To develop an approach to analyze Sentinel–2 satellite data using traditional and principal component analysis based approaches to create land use and land cover map, which is a prerequisite for developing the curve number. **Error! Bookmark not defined.**
 3. **Objective:** To perform Morphometrical analysis of Vishwamitri watershed and prioritization of sub-watersheds for assessing the flood influencing characteristics of the sub-watersheds of the Vishwamitri watershed. **Error! Bookmark not defined.**
 4. **Objective:** To identify potential runoff storage zones based on the various physical characteristics of the Vishwamitri watershed using a GIS-based conceptual framework that combines through analytic hierarchy process using multi criteria decision-making method..... **Error! Bookmark not defined.**
 5. **Objective:** To develop an approach for operational flood extent mapping using Synthetic Aperture Radar (SAR) and preparation of flood inundation map for data scarce region using 2D flow modelling using rain on grid model. **Error! Bookmark not defined.**
 6. **Objective:** To quantify the effects of urban land forms on land surface temperature and modeling the spatial variation using machine learning. **Error! Bookmark not defined.**
6. **Conclusions and Recommendations** **Error! Bookmark not defined.**
 - 6.1 **General**..... **Error! Bookmark not defined.**
 - 6.2 **Conclusions** **Error! Bookmark not defined.**
 - 6.3 **Recommendations**..... **Error! Bookmark not defined.**
7. **References** **Error! Bookmark not defined.**

Table of Contents of executive summary

1. Methodology	1
1.1. General	1
1.2. Methodology	1
1. Objective: To demonstrate a comparative assessment of discrepancy in the hydrological behaviour of the DEMs in terms of terrain representation at the catchment scale.	1
2. Objective: To develop an approach to analyze Sentinel–2 satellite images using traditional and principal component analysis based approaches to create land use and land cover map, which is a prerequisite for developing the curve number.	2
3. Objective: To perform Morphometrical analysis of Vishwamitri watershed and prioritization of sub-watersheds for assessing the flood influencing characteristics of sub-watersheds of the Vishwamitri river.....	4
4. Objective: To identify potential runoff storage zones based on the various physical characteristics of the Vishwamitri watershed using a GIS-based conceptual framework that combines through analytic hierarchy process using multi criteria decision-making method. ...	5
5. Objective: To develop an approach for operational flood extent mapping using Synthetic Aperture Radar (SAR) and preparation of flood inundation map for data scarce region using 2D flow modelling using rain on grid model.	6
6. Objective: To quantify the effects of urban land forms on land surface temperature and modeling the spatial variation using machine learning. The models can help to predict land surface temperature under temporary cloud cover spots, which are present in the data at the time of the acquisition, using neighboring biophysical (cloud-free) independent variables relationship with land surface temperature.	8
2. Results and analysis	10
2.1 General	10
2.2 Results and analysis	10
1. Objective: To demonstrate a comparative assessment of discrepancy in the hydrological behaviour of the DEMs in terms of terrain representation at the catchment scale.	10
2. Objective: To develop an approach to analyze Sentinel–2 satellite data using traditional and principal component analysis based approaches to create land use and land cover map, which is a prerequisite for developing the curve number.	10
3. Objective: To perform Morphometrical analysis of Vishwamitri watershed and prioritization of sub-watersheds for assessing the flood influencing characteristics of the sub-watersheds of the Vishwamitri watershed.	11
4. Objective: To identify potential runoff storage zones based on the various physical characteristics of the Vishwamitri watershed using a GIS-based conceptual framework that combines through analytic hierarchy process using multi criteria decision-making method.	12
5. Objective: To develop an approach for operational flood extent mapping using Synthetic Aperture Radar (SAR) and preparation of flood inundation map for data scarce region using 2D flow modelling using rain on grid model.	17

6. Objective: To quantify the effects of urban land forms on land surface temperature and modeling the spatial variation using machine learning. The models can help to predict land surface temperature under temporary cloud cover spots, which are present in the data at the time of the acquisition, using neighboring biophysical (cloud-free) independent variables relationship with land surface temperature.....	19
3. Conclusions and Recommendations	22
3.1 General	22
3.2 Conclusions	22
3.3 Recommendations	25
7. References	29

1. Methodology

1.1. General

This chapter shows the methodology adopted for the individual objectives. The chapter is divided into six sections, each section contains the specific methodology for the specific objective.

1.2. Methodology

1. **Objective:** To demonstrate a comparative assessment of discrepancy in the hydrological behaviour of the DEMs in terms of terrain representation at the catchment scale.

To evaluate the sensitivity of data sources and their vertical accuracies, two hydrologic applications, watershed boundary and river network extraction, are used along with various statistical measures. Hydrologic applications are selected because they heavily rely on DEM data. The workflow is divided into following three steps:

Datum Transformation: Datum transformation is carried out to bring the DEMs to common horizontal datum and vertical datum. SRTM and ASTER data are referenced to WGS84 horizontal datum and EGM96 vertical datum. But, the ellipsoidal height of terrain (in meters), with WGS84 ellipsoid as a horizontal and a vertical datum, in Geographic Projection System (i.e., X and Y in terms of latitude and longitude) is provided by Cartosat DEM. So, the Cartosat DEM has been reprojected by using the Vdatum transformation tool provided by NOAA's National Ocean Service in a Geographic (lat./long.) projection, to WGS84 as a horizontal datum and EGM96 as a vertical datum.

Visual Comparison: The aim of visual comparison was to detect changes between the results, such as streams and watershed derived from the different DEMs by using the shaded relief map and the high-resolution satellite imagery. The Vishwamitri watershed was selected for heterologous comparison of slope maps, ridge lines and streams generated by ASTER, SRTM, and Cartosat DEMs. The maximum rate of change of the elevation of the plane (the angle that the plane makes with a horizontal surface) is called the slope gradient. A declivity map with a pixel size of 30 m was created for analyzing the influence of the terrain slope on the models. Watershed delineation was performed by GIS software by importing DEMs. A pixel or a set of spatially connected pixels whose flow direction cannot be assigned to one of the eight valid values in a raster of the flow direction is called a sink. In order to remove small imperfections in the data, the Fill Sink tool was used. Sinks must be filled to ensure a proper delineation of basins and streams. A derived drainage network may be discontinuous if the sinks are not filled. A raster of the flow direction from each pixel to its downslope neighbours is created by the flow-

direction tool. The accumulated flow as the accumulated weight of all pixels flowing into each downslope pixel in the output raster is calculated by the flow accumulation tool. Pixels with a high flow accumulation are termed as areas of concentrated flow, which may be used for identifying stream channels. Similarly, pixels with a flow accumulation of 0 are termed as local topographic highs, which may be used for identifying ridges. A stream network can be delineated by applying a threshold value to the flow accumulation raster. A user-defined and important parameter, which is known as the stream threshold, directly affects the drainage network and basin boundaries that would be obtained by hydrological analysis. In this study, the stream threshold has been considered as 1% of the maximum flow accumulation value (Paul et al., (2015)). The point on the surface at which water flows out of an area is called the outlet or the pour point. The outlet is the lowest point along the boundary of a watershed. Figure 4.1 shows the methodology adopted for watershed delineation. Map algebra that determines where the Fill tool had filled the sinks was used to investigate the cause of the errors in the streams network.

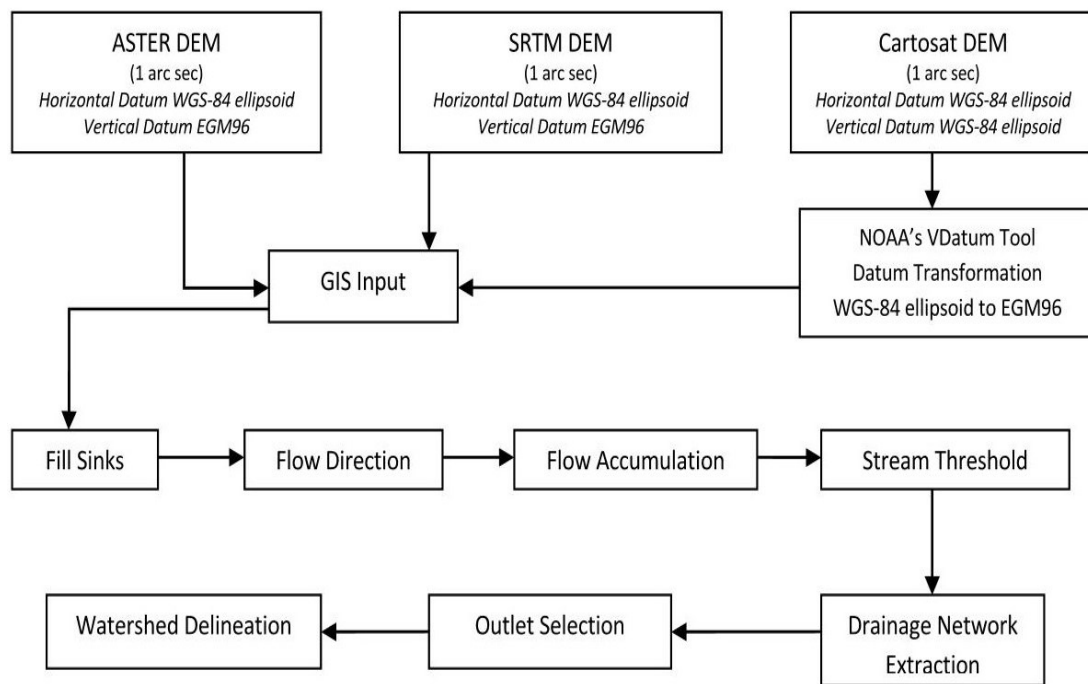


Figure 4.1: Methodology adopted for watershed delineation.

2. **Objective:** To develop an approach to analyze Sentinel-2 satellite images using traditional and principal component analysis based approaches to create land use and land cover map, which is a prerequisite for developing the curve number.

The Sentinel-2 cloud-free Level 1C data product (L1C_T43QCE_A008039_20180920T054434) acquired on 20 September 2018 was downloaded from the Sentinel Hub developed by European Space Agency. Sentinel-2 Level 1C data were processed from Top-Of-Atmosphere Level 1C to

Bottom-Of-Atmosphere Level 2A. QGIS desktop 3.6.1 is a free and open-source cross-platform desktop geographic information system application that supports viewing, editing, and analysis of geospatial data. QGIS desktop 3.6.1 interface was used with Semi-Automatic Classification Plugin (SCP), to convert the Sentinel-2 MSI data to reflectance values and for dark object subtraction atmospheric correction (DOS1) of the data. After atmospheric correction, ten bands (2-8, 8A, 11 and 12) were composited and clipped to the study area. The processed data were georeferenced to the WGS 84 UTM 43N projected coordinate system. In order to test the effectiveness of PCA, two stacks were created for the classification in ESRI's ArcGIS Desktop 10.5 software. Stack 1 contained atmospherically corrected bands (2-8, 8A, 11 and 12) and Stack 2 contained 3 major PCA bands accounting for the 97.96% of eigenvalues. The PCA technique was used to reduce the number of bands or dimensions necessary for classification. Dimension reduction leads to a reduction in the computation costs without compromising the desired variability in the data. According to [Mather, \(2010\)](#) the process of PCA can be divided into three steps. The first step is to calculate the covariance or correlation matrix of multiband images. The covariance matrix is calculated by [Eq. \(1.2\)](#).

$$C_{XY} = \frac{\sum_{i=1}^n (X_i - \bar{X})(Y_i - \bar{Y})}{n-1} \quad 1.2$$

- C_{XY} = Covariance between Band X and Band Y
- n = The number of pixels
- X_i = Individual pixel value vectors of Band X
- \bar{X} = Mean of Band X
- Y_i = Individual pixel value vectors of Band Y
- \bar{Y} = Mean of Band Y

The diagonal elements of the covariance matrix are the band variances, and the off-diagonals are band covariances. If a correlation matrix is used instead of a covariance matrix, each entry in C should be further divided by the product of the standard deviations of the features represented by the corresponding row and column.

$$R_{XY} = \frac{C_{XY}}{\sigma_X \sigma_Y} \quad 1.3$$

- R_{XY} = Correlation between Band X and Band Y
- C_{XY} = Covariance between Band X and Band Y
- σ_X = Standard deviations of Band X
- σ_Y = Standard deviations of Band Y

The second step is to calculate the eigenvectors of the covariance matrix. Following equation is used for the calculation:

$$(C - \lambda_i I)A_i = 0 \quad 1.4$$

C = Covariance matrix
 λ_i = Eigenvector
 I = Identity matrix
 A_i = Eigenvalue

The normalized eigenvectors of the covariance or correlation matrix form the new coordinate system. The mapping location f_i of each pixel $X=(x_1, x_2, \dots, x_k)$ on the i^{th} principal component is given by:

$$f_i = XA_i = x_1 a_{1i}, x_2 a_{2i}, \dots, x_k a_{ki} \quad 1.5$$

which shows the rotation of the axes of the feature space.

The traditional approach and PCA based approach used Stack 1 and Stack 2, respectively, as inputs for land use and land cover classification. The training data were collected based on the manual interpretation of the original Sentinel-2 data and DigitalGlobe's WorldView-4 high-resolution imagery and was kept the same for all the three classifiers to avoid the optimistic bias in classification. The training sample size was kept below 1000 pixels per class to evaluate the influence of the training sample size, as well as the performance of classification algorithms. Training data for each land use and land cover class were collected as a group of pixels. The input data and corresponding ground truth data (training sample) were used to train the classifiers. The classifiers learn the complex relationships between the input and ground truth data (training sample). To determine the accuracy of each classification and class, thematic accuracy assessment was performed. For this purpose, firstly a reference data set including a total of 100 points was created. Stratified random sampling was used with 100 points to obtain the ground truth data from the manual interpretation of the original 10 m resolution Sentinel-2 data (Band 2, 3 and 4) and DigitalGlobe's WorldView-4 data (Product Id: 1ba34688-3ee0-41e4-9187-de68fdb075df-inv) acquired on 25-10-2018 at 5:30 am with 31 cm resolution. The results of the classifications were not post-processed (e.g., filtered). The classification maps were evaluated in terms of their overall accuracy (OA), producer's accuracy (PA), user's accuracy (UA) and the Kappa index of agreement (k) or Kappa coefficient and a Confusion matrix was created.

- 3. Objective:** To perform Morphometrical analysis of Vishwamitri watershed and prioritization of sub-watersheds for assessing the flood influencing characteristics of sub-watersheds of the Vishwamitri river.

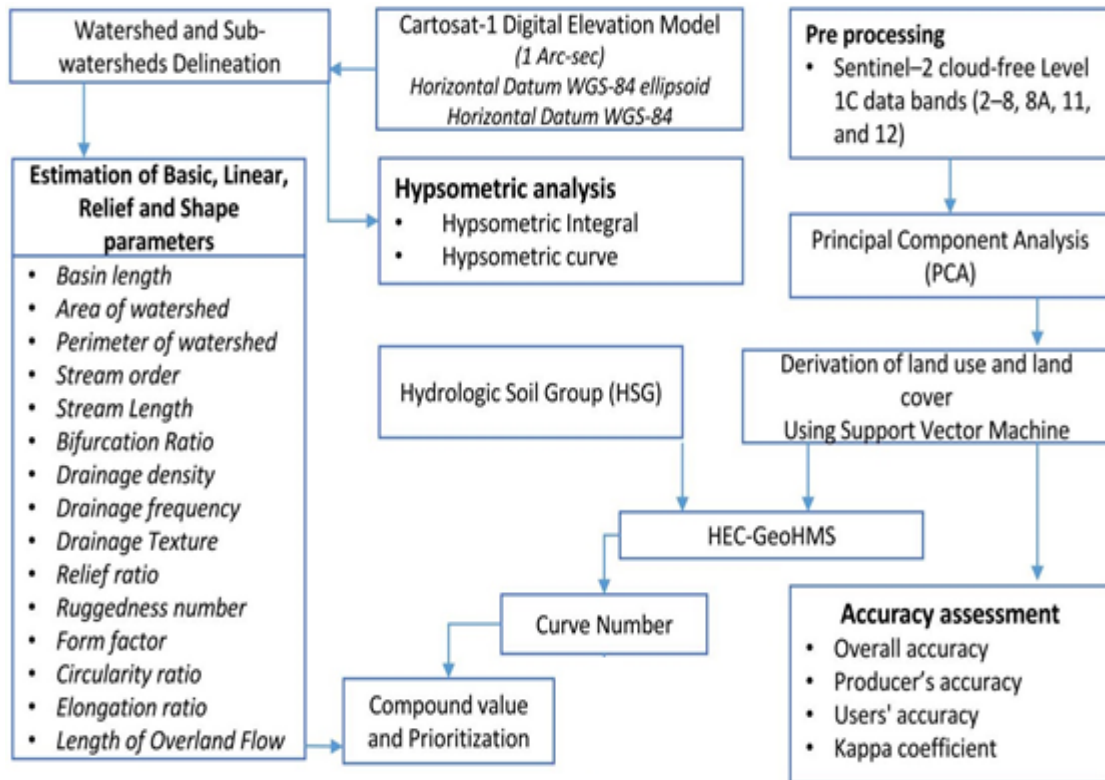


Figure 4.4: Methodology adopted for prioritization of sub-watersheds for assessing the flood influencing characteristics of sub-watersheds.

4. Objective: To identify potential runoff storage zones based on the various physical characteristics of the Vishwamitri watershed using a GIS-based conceptual framework that combines through analytic hierarchy process using multi criteria decision-making method.

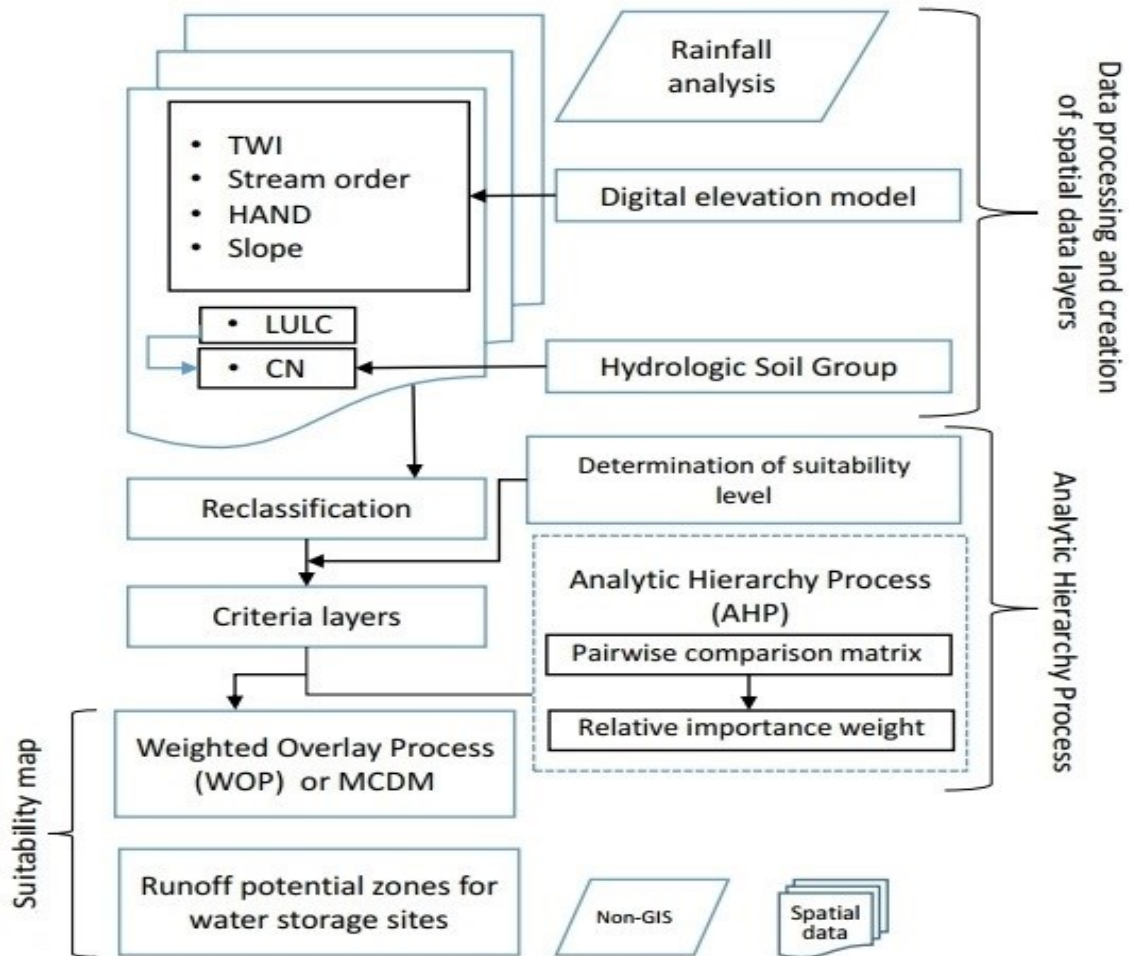


Figure 4.6: Multi criteria decision making (MCDM) technique workflow using AHP for identification of potential runoff storage zones for water storage.

- 5. Objective:** To develop an approach for operational flood extent mapping using Synthetic Aperture Radar (SAR) and preparation of flood inundation map for data scarce region using 2D flow modelling using rain on grid model.

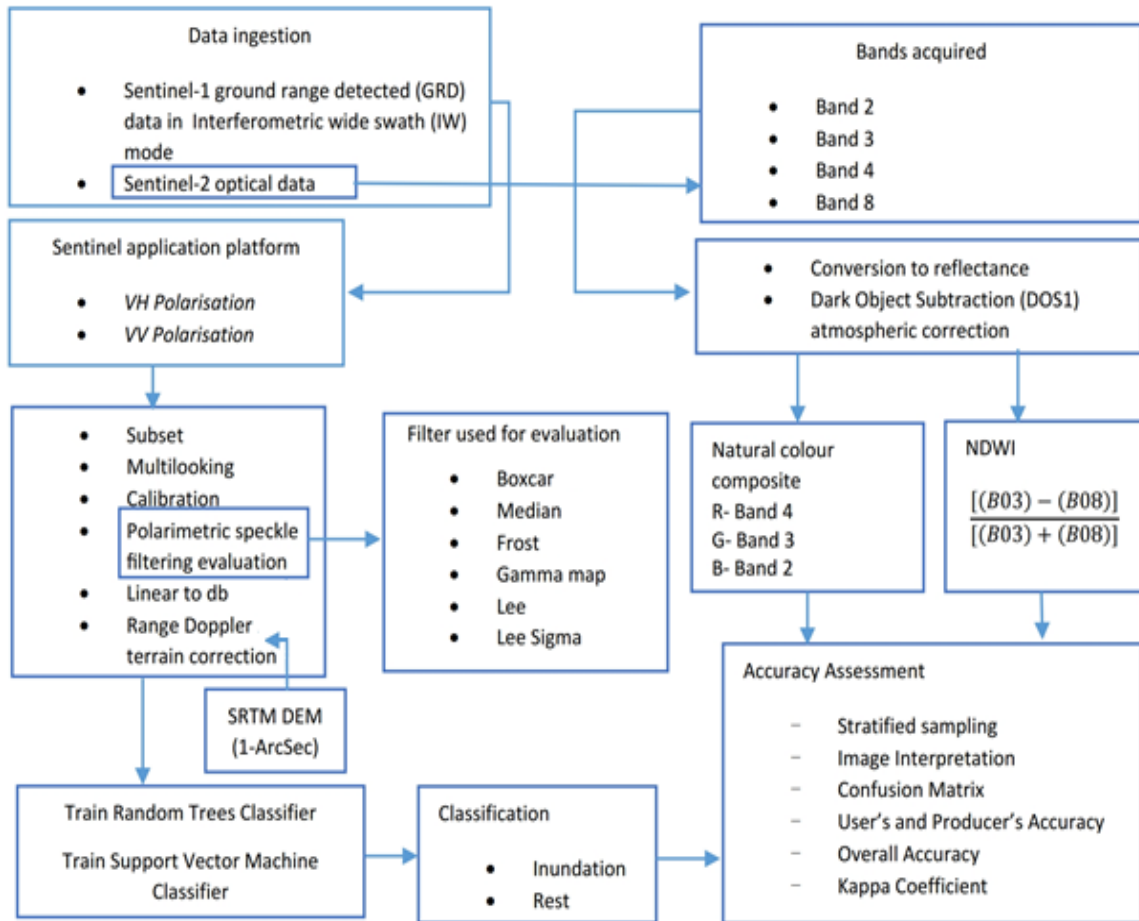


Figure 4.9: Methodology of SAR workflow.

2D Hydraulic modelling for flood hazard assessment:

The intent of this work is to examine the findings of situations for which no observed data or very limited data, related to flooded areas and discharge, are available. This is a common occurrence in small watersheds, which are frequently ungauged catchments for which data for model calibration and validation is unavailable (Costabile et al., (2020)). In circumstances like these, the reliability of the commercial applications should be measured using a state-of-the-art research model that is developed for benchmarking purposes. For these reasons, an observed storm event (30-07-2019 to 03-08-2019) for modelling has been taken under study. This period of storm event witnessed the stronger than normal cross equatorial flow and active monsoon conditions over major parts of the watershed during last week of July to first phase of August in the year 2019. For rainfall-runoff simulations at the watershed scale, the runoff was evaluated with the well-known SCS-CN method, the potential maximum soil retention is calculated using following formula:

$$S = \frac{25400}{CN} - 254 \quad 4.27$$

Where, S is in mm, and CN is the curve number (dimensionless).

The assumption of SCS-CN is that, for a single storm event, potential maximum soil retention is equal to the ratio of direct run-off to available rainfall. This relationship, after algebraic manipulation and inclusion of simplifying assumptions, results to the following expression:

$$\text{Daily Runoff (mm), } Q = \frac{(P - I_a)^2}{(P + S - I_a)} = \frac{(P - \lambda S)^2}{P + (1 - \lambda)S} \text{ for } P > \lambda S \quad 4.28$$

Q = direct run-off depth

P = total rainfall

I_a = initial abstraction

I_a and S can be related using the following equation:

$$I_a = \lambda S$$

λ = 0.2 was assumed in original SCS-CN model

The Hydrologic Engineering Center's Geospatial Hydrologic Modeling Extension (HEC-GeoHMS) is extension to ESRI's ArcGIS software that compute the curve number and other loss rate parameters based on various soil and land use/land cover databases. HEC-GeoHMS is used to create the curve number with the help of the Support Vector Machine classified land use and land cover map using Principal Component Analysis (PCA) based approach and soil map containing hydrological soil groups. One of the most popular and most used model in both the scientific literature and in practice amongst the software packages using physically oriented equations. The Hydrologic Engineering Centre-River Analysis System (HEC-RAS) developed by the U.S. Army Corps of Engineers. In the latest release version (5.0.7), the HEC-RAS model is complimented by new modules, which include complete 2-D calculations based on 2-D fully dynamic equations and 2-D diffusion wave equations that ignore inertial conditions. It also provides the possibility of 1-D/2-D combined simulations, which aim to combine both a full 2-D and a full 1-D.

6. **Objective:** To quantify the effects of urban land forms on land surface temperature and modeling the spatial variation using machine learning. The models can help to predict land surface temperature under temporary cloud cover spots, which are present in the data at the time of the acquisition, using neighboring biophysical (cloud-free) independent variables relationship with land surface temperature.

The methodology used in the study is presented in [Figure 4.11](#). The workflow was divided into six steps. First, the satellite data were subjected to image pre-processing and atmospheric correction to remove the atmospheric effect and sensor defects for land surface temperature retrieval. Second, the classification of the heat zones. Third, derivation of land use/land cover

and accuracy assessment. Fourth, derivation of NDVI, NDWI and DBSI. Fifth, calculate Land Contribution Index (CI) and Landscape index (LI). Sixth, model fitting and evaluation.

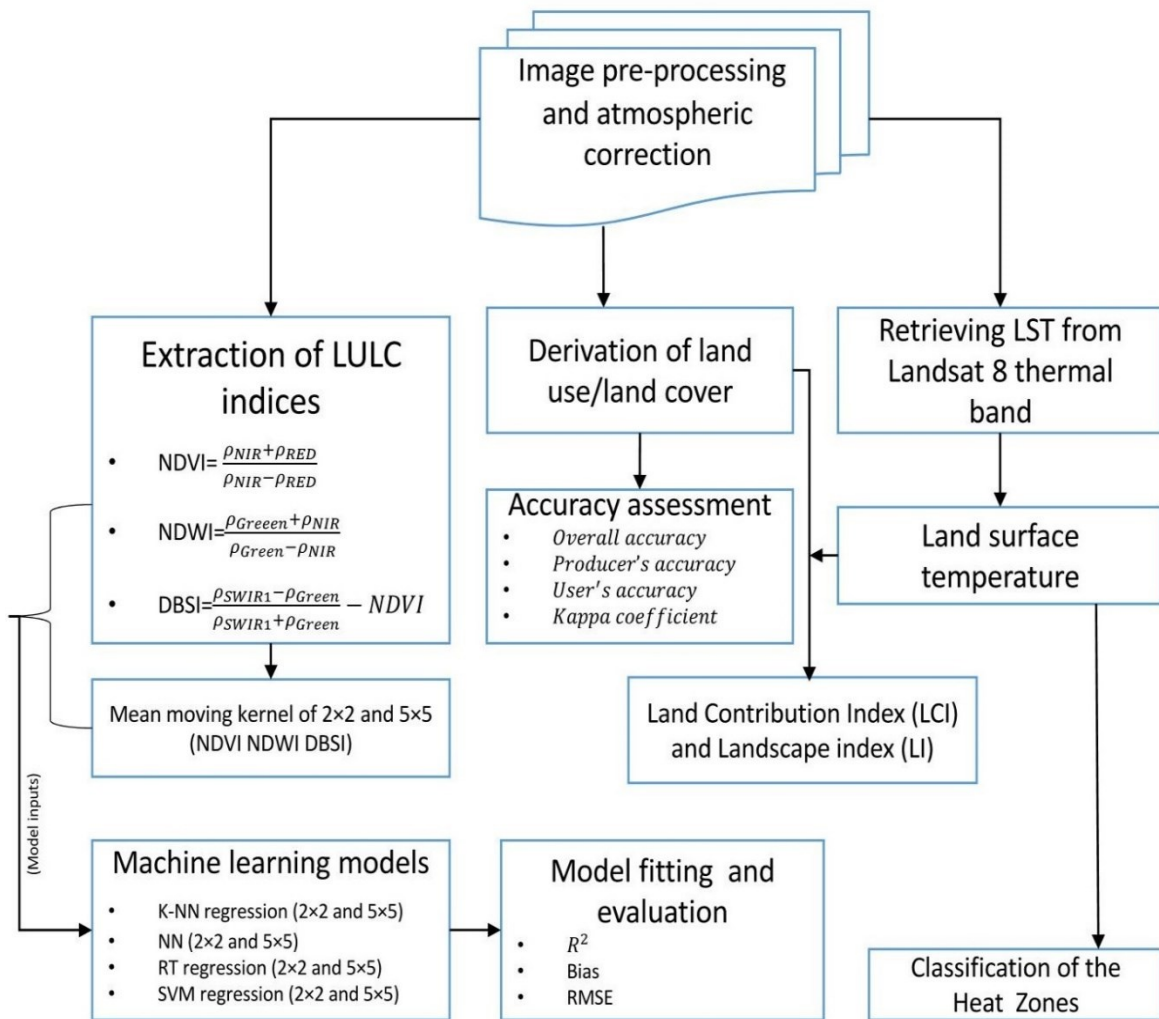


Figure 4.11: Methodology adopted to quantify the effects of urban land forms on land surface temperature and modeling the spatial variation using machine learning.

2. Results

2.1 General

This chapter shows the results obtained for the individual objectives, based on the results obtained the analysis has been carried out. The chapter is divided into six sections, each section contains the results obtained for the specific objective.

2.2 Results

1. **Objective:** To demonstrate a comparative assessment of discrepancy in the hydrological behaviour of the DEMs in terms of terrain representation at the catchment scale.

A comparison of SRTM-, ASTER-, and Cartosat-derived DEMs allowed a qualitative assessment of the vertical component of the error, whereas statistical measurements were used to estimate their vertical accuracy. In order to compare the frequency histograms of the elevation distributions in the DEMs in the study area, skewness and kurtosis were determined. Further, to obtain the degree of relationship between the DEMs, scatterplots, as well as correlation coefficients, were used. The results showed that all DEMs have imperfections in the delineation of a small river like Vishwamitri, and the comparison showed that SRTM 30 m and ASTER 30 m failed to delineate proper main drainage for the river. Cartosat 30 m DEM exhibited better results. The root mean square error (RMSE) was calculated as 7.21 m for ASTER and 3.24 m for SRTM. The correlation value of 0.94 indicates the existence of a strong positive linear correlation between SRTM and Cartosat. The study shows that for the study area ASTER elevation data were highly underestimated, whereas SRTM elevation data were slightly overestimated.

2. **Objective:** To develop an approach to analyze Sentinel-2 satellite data using traditional and principal component analysis based approaches to create land use and land cover map, which is a prerequisite for developing the curve number.

The overall classification accuracy varied considerably among the classifiers. The overall classification accuracy of MLE classifier was increased from 22% to 41% (19% increase) in the PCA based approach. The overall accuracy RF classifier was increased by 10% reaching 70%, whereas SVM classifier outperformed both the classifiers with 76% overall accuracy (increased by 12%). Spectral response curve is the curve showing the variation of reflectance or emittance (in terms of Digital numbers) of a material with respect to wavelengths. Figure 5.14 81 (b) and 5.15 (b) show the variation of responses of the land use and land cover classes in Stack 1 and Stack 2 respectively. Classes having similar responses are hard to separate. It was also observed that as the spectral distance (or separability) of the classes Water and Built-up in Stack 1 and

Stack 2 (Figure 5.14 (b) and 5.15 (b)) in relation to other classes was more, that is why the user's accuracy (UA) and producer's accuracy (PA) for water and Built-up classes are high, for both traditional and PCA-based classification approaches. Kappa coefficient showed a similar trend as that of the overall accuracy. Overall accuracy is calculated by the proportion of the correctly classified pixels to the total number of pixels. Highest Kappa coefficient values were obtained with SVM in PCA based approach followed by the RF.

- 3. Objective:** To perform Morphometrical analysis of Vishwamitri watershed and prioritization of sub-watersheds for assessing the flood influencing characteristics of the sub-watersheds of the Vishwamitri watershed.

Watershed morphometry reveals lumped or semi-distributed watershed features. Watershed hydrology is highly influenced by its morphometry. Runoff potential is directly related to a variety of morphometrical parameters including drainage density, drainage frequency, mean bifurcation ratio, drainage texture, and elongation ratio (i.e., the greater the values of these parameters, the greater the watershed's runoff potential and vice versa). Morphometric parameters were directly calculated from the Cartosat-1 30m DEM by using Arc-hydro tools. Morphometry of Vishwamitri watershed and sub-watersheds, and its hydrological importance are discussed in detail below.

I. Compound value and weightage:

Single or limited parameters cannot present a comprehensive picture of the flood hazard potential of any sub-watershed, and hence, each of the linear, aerial, and relief morphometric parameters along with curve number is taken into consideration for assessing the flood influencing characteristics of the five sub-watersheds of the Vishwamitri watershed, as these parameters have a direct but variable relationship with flood runoff. Therefore, influencing value or rank (highest weightage 5 and least 1) is given to each sub-watershed based on the nature of the selected parameter. Prioritization was achieved through the allocation of weights to the individual indicators contributing to flood runoff and a compound value (C_v) was calculated for final prioritization. C_v is derived by calculating the average of ranks assigned to the individual parameters. The sub-watershed with highest C_v contributes most to flood runoff and as a result needs highest priority for flood mitigation measures, whereas the sub-watershed with lowest C_v is contributing least to flood runoff thereby has low priority. Thus an index of high, medium and low priority was produced. Based on the integration of each flood influencing parameter and calculated compound value, the SW I and IV areas of Vishwamitri watershed have been categorized into high priority, SW II and V into moderate priority, and SW III into low

priority. In order to mitigate floods, it is proposed that there is a significant need to create a flood spill channel that can take up to one-third of the total flow of the Vishwamitri river. Moreover, to prevent floods in the downstream agricultural areas and settlements, an additional reservoir must be created in SW I. Along with this, mitigation measures such as, check dams, nala bunds, gully plug, bundhis (local name in India), percolation tanks, etc. can be constructed in a planned and systematic manner in SW I, II and IV to create water buffers within the catchment, which will help reducing vulnerability to seasonal variations in rainfall. Nala bunds and percolation tanks are structures built across or closer to nalas (streams) to increase water percolation, increase the moisture regime of the soil, and restrict silt flow.

- 4. Objective:** To identify potential runoff storage zones based on the various physical characteristics of the Vishwamitri watershed using a GIS-based conceptual framework that combines through analytic hierarchy process using multi criteria decision-making method.

Determining criteria weights using AHP

AHP provided a systematic approach to conduct MCDM. To derive suitability maps for potential runoff storage zones, the criteria maps have to be related to the result of the AHP. The AHP pair-wise matrix for the criteria used in this study is presented in [Table 2.1](#). For all the five spatial layers the relative importance is derived. Thus, a common scale (0 % to 100 %) is obtained from AHP procedure. As seen in [Table 2.1](#), the most important criterion for decision-making is Slope (22.50%), followed by LULC (21.20%), Curve number (14.80%), HAND (14.50%), Stream order (14.40%) and TWI (12.60%). Calculated principal eigenvector is 6.47, which is computed with the square reciprocal matrix of pairwise comparisons between criteria. Since the AHP may have inconsistencies in establishing the values for the pairwise comparison matrix, it is important to calculate this level of inconsistency using the consistency ratio (CR) ([Rincón et al., \(2018\)](#)). The CR of the pair-wise matrix is 7.5% (which is less than 10 %) and thus the judgments made and compiled in the pair-wise matrix of [Table 2.1](#) are acceptable. This implies that the comparisons were performed with good judgment, weightage for each criterion is suitable to weighted overlay.

Table 2.1: Resulting weights for the criteria based on pairwise comparisons.

	Slope Based on TPI	TWI	LULC	Curve number	Stream order	HAND	Priority	Rank
Slope Based on TPI	1	2	0.5	2	2	2	22.50%	1
TWI	0.5	1	1	1	1	0.5	12.60%	6
LULC	2	1	1	1	2	1	21.20%	2
Curve number	0.5	1	1	1	0.5	2	14.80%	3
Stream order	0.5	1	0.5	2	1	1	14.40%	5
HAND	0.5	2	1	0.5	1	1	14.50%	4

Weighted Overlay Process (WOP) within GIS

Potential runoff storage zones of the study area (Figure 2.1) was generated by integrating the thematic layers of slope, LULC, curve number, HAND, stream order and TWI using weighted overlay process (WOP) within GIS. Resulted raster was classified into four classes namely (a) Not suitable (b) Marginally Suitable (c) Moderately Suitable (d) Optimally Suitable. Result shows that 17 % of the area is optimally suitable, 33.2% of the area is moderately suitable, 33.1 % of the area is marginally suitable and 18.7% of the area is not suitable for water storage zones/structures. Sixteen suitable sites on such zones (optimally suitable class) have also been identified for water storage structures, as shown in Figure 2.2. Criteria of selection of these sites are: first, proximity of the sites to the agricultural fields. Second, sites should be on unused or barren land. Third, narrow cross-section of the valley with high shoulders to minimise the amount of construction material needed for building the small dams or check dams, nala bunds, gully plug and bundhis. Results are also confirmed by the already built water storage structures in derived potential runoff storage zones which are in optimally suitable class (Figure 2.3).

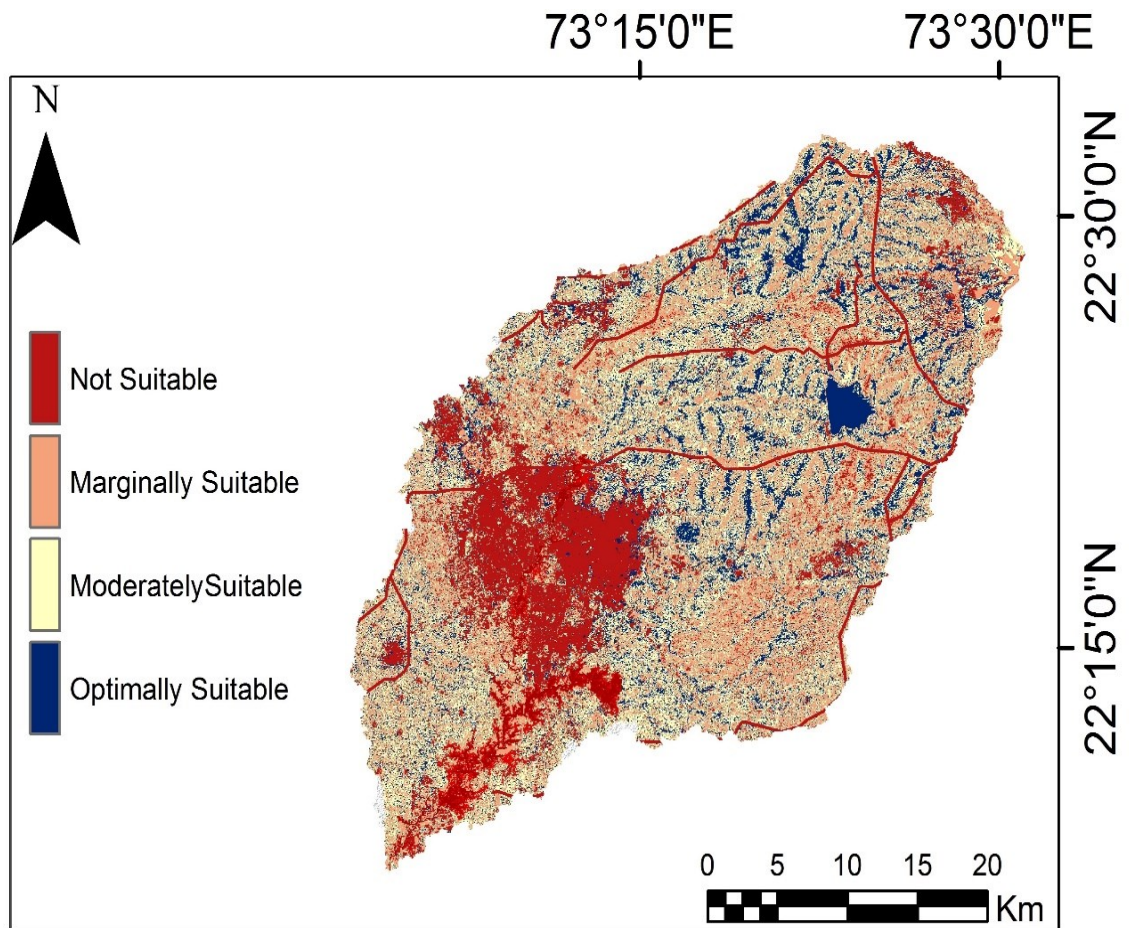


Figure 2.1: Potential runoff storage zones of the study area.

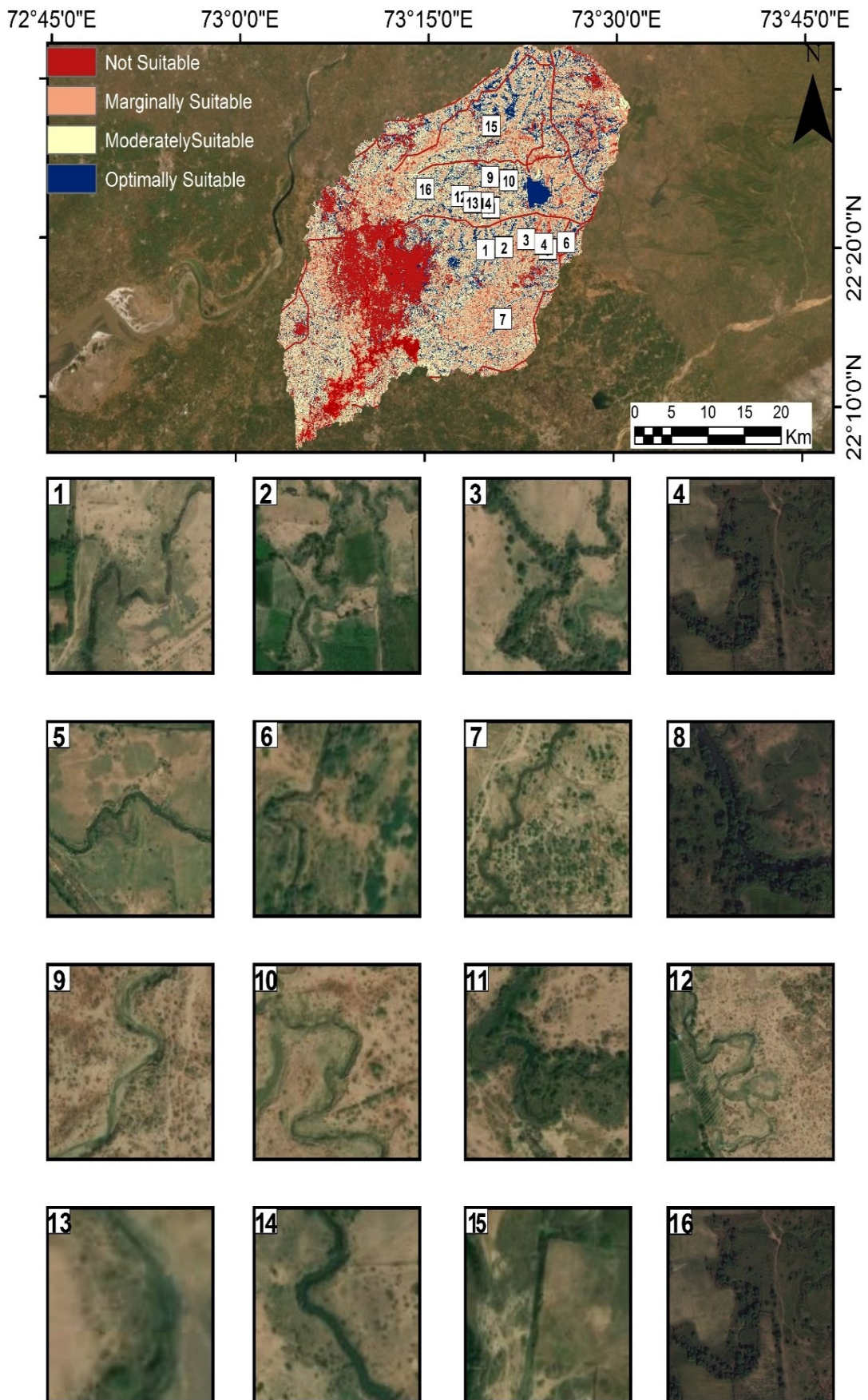


Figure 2.2: Identified sites for water storage structures on potential runoff storage zones.

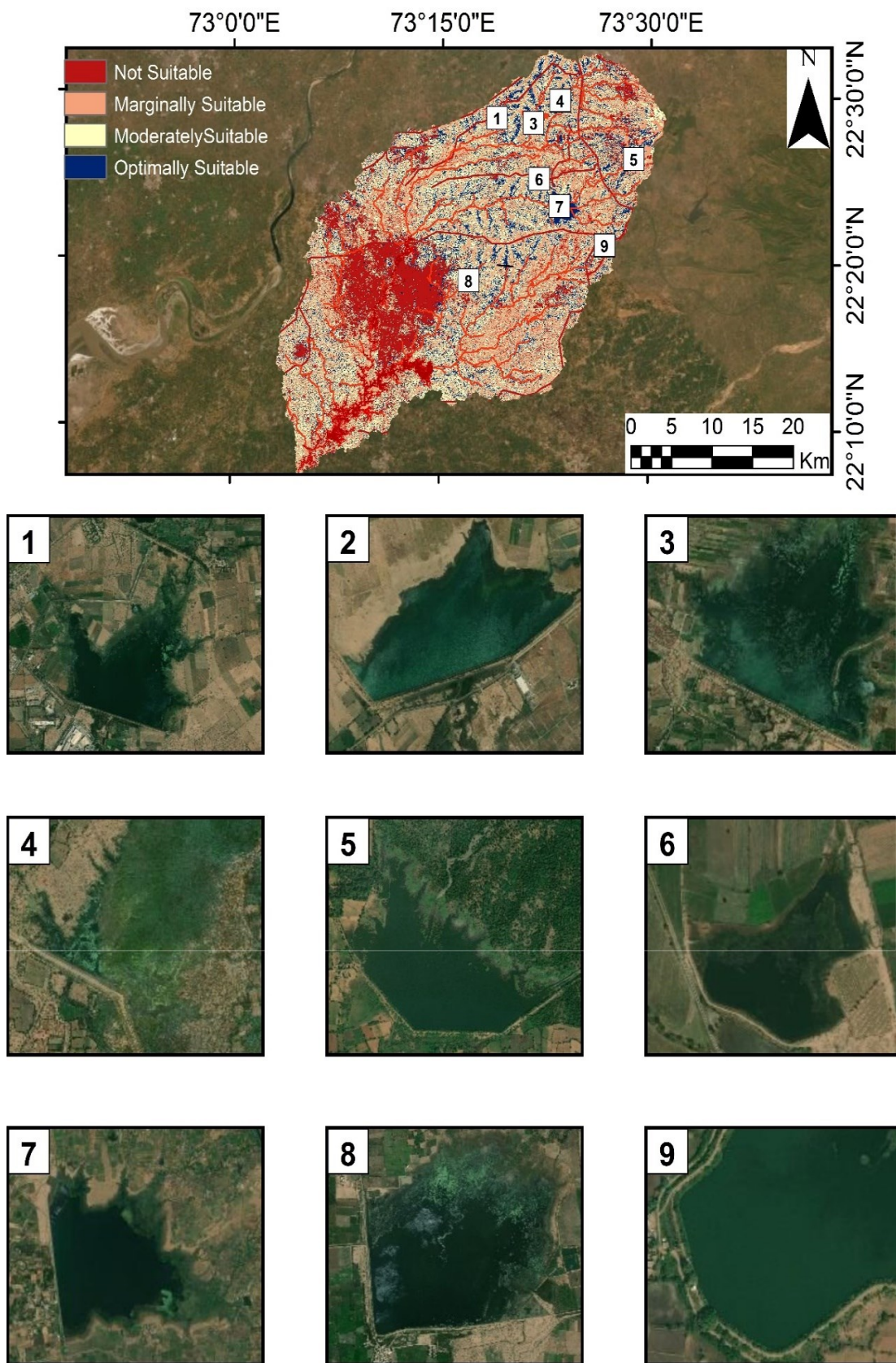


Figure 2.3: Already built water storage structures on the derived potential runoff storage zones.

5. Objective: To develop an approach for operational flood extent mapping using Synthetic Aperture Radar (SAR) and preparation of flood inundation map for data scarce region using 2D flow modelling using rain on grid model.

For the study area Kerala, the random forest classifier exhibited maximum overall accuracy of 88.80% with the kappa coefficient value of 0.72. Both the classifiers obtained better accuracy results in VV polarization compared to the VH polarization. The least overall accuracy of 82.60% and a kappa coefficient value of 0.63 were observed with random forest in VH polarization, which was followed by the support vector machine in VV polarization. RF achieved higher classification accuracy than SVM by about 5% in VV polarization. However, both the classifiers produced comparable overall accuracies in VH polarization (SVM achieved higher classification accuracy than RF by about 1%). The inundated area in the calculated NDWI over the cloud-free extent is 73.88%, which is 41.78 km². However, it has also been observed that the inundated area using random forest classification on filtered VV data over the cloud-free extent is 71.18%, which is 40.25 Km². For the study area Assam, the SVM classifier exhibited maximum overall accuracy of 92% with the kappa coefficient value of 0.81. Both the classifiers obtained better accuracy results in VH polarization compared to the VV polarization. The least overall accuracy of 83.60% and a kappa coefficient value of 0.65 were observed with random forest in VV polarization, which was followed by the RF in VH polarization. SVM achieved higher classification accuracy than RF by about 5.38% in VH polarization. The inundated area in the calculated NDWI over the cloud-free extent is 74.09%, which is 491.47 km². However, it has also been observed that the inundated area using SVM classification on filtered VH data over the cloud-free extent is 62.76%, which is 416.99Km². To calculate inundation for the entire scene, threshold value of -10.96 and -19.58 was selected for Kerala and Assam region respectively after analysing the histograms. The calculated inundated area with thresholding technique for Kerala was found 204 km² (2% more than classified VV polarised data using RF algorithm). Similarly, the calculated inundated area with thresholding technique for Assam was found 3368.90 km² (23.46% more than classified VH polarised data using SVM algorithm). For Assam region the variation is very large, a single threshold did not hold well as large swath of a SAR image suffers from environment heterogeneity caused by wind-roughening and satellite framework parameters.

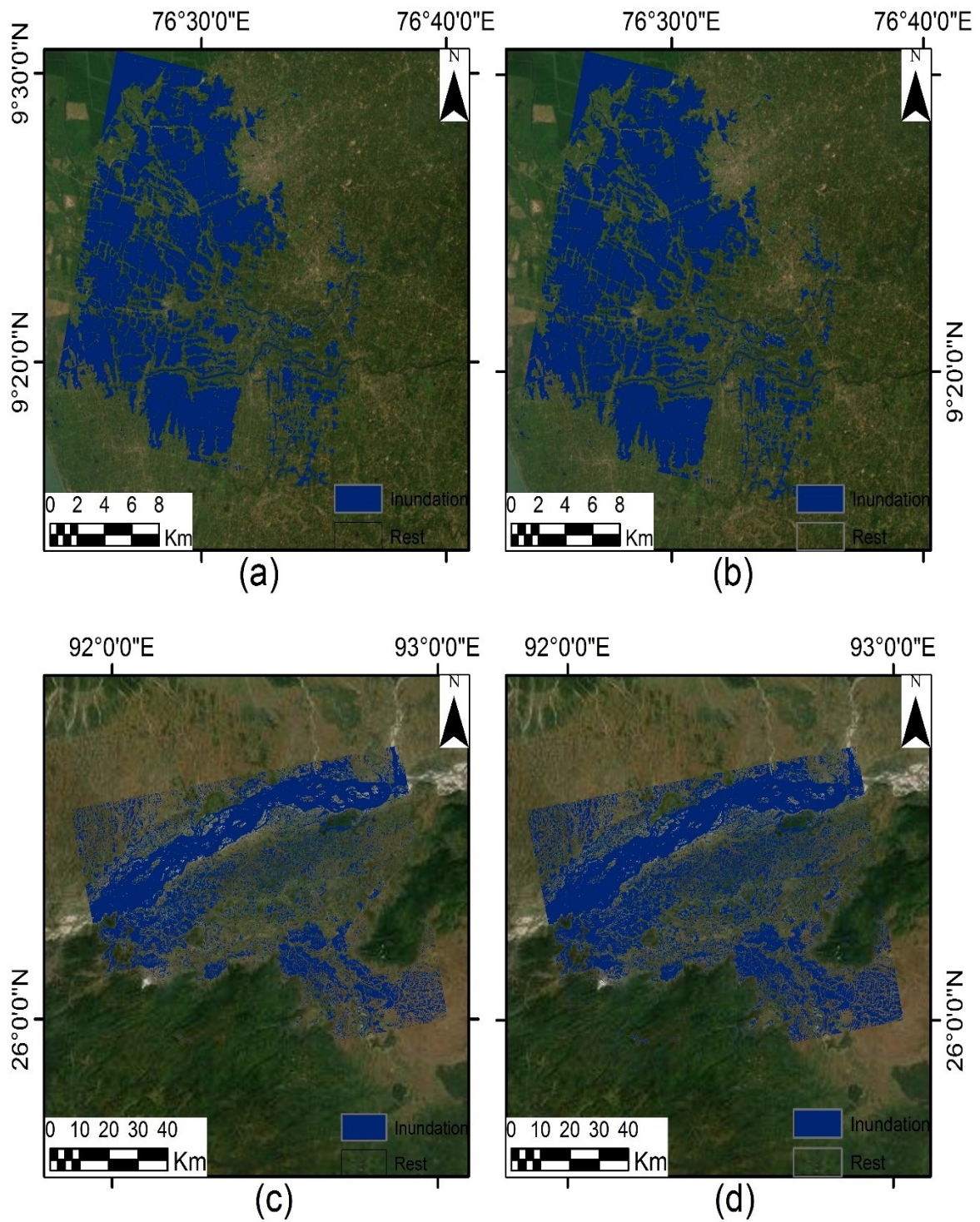


Figure 2.4: (a) Random forest tree classification on filtered VV data (Kerala) (b) Classified filtered VV data with threshold value of -10.96 (Kerala) (c) Support vector machine classification on filtered VH data (Assam) (d) Classified filtered VH data with threshold value of -19.58 (Assam).

A. 2D hydraulic modelling for inundation:

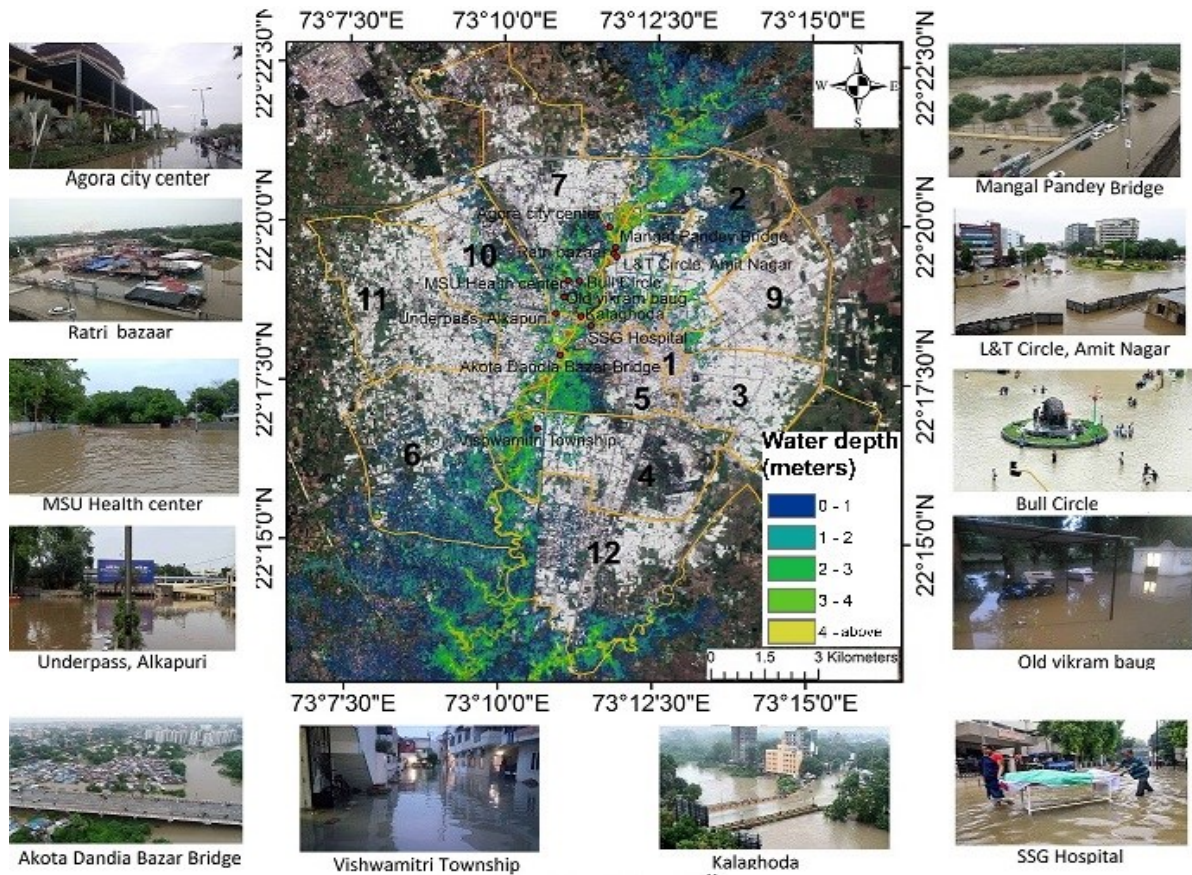


Figure 2.5: Inundation map of Vadodara city with sites visit

6. Objective: To quantify the effects of urban land forms on land surface temperature and modeling the spatial variation using machine learning. The models can help to predict land surface temperature under temporary cloud cover spots, which are present in the data at the time of the acquisition, using neighboring biophysical (cloud-free) independent variables relationship with land surface temperature.

Temperature Variations for Different Land Cover Types

To understand the relationship between land surface temperature and land use/land cover, the investigation of the thermal signature of each land use/land cover form is important. A comparison was therefore carried out between land use/land cover and land surface temperature. The mean temperature of each landform category was calculated by averaging all consistent pixels of a given landform category. The average LST at 11:02:51.19 AM in summer reached up to 41.0 °C, whereas in winter it was 30.9 °C.

The average land surface temperature values of four land use/land cover types from high to low are baresoil > builtup > vegetation > water. The results indicated the highest land surface temperature was recorded for baresoil while the lowest was recorded for water bodies for both the seasons. In the study period, the city of Vadodara showed lower surface temperatures in residential urban areas as compared to the outskirts of the city. It is caused by heat from the sun in the surrounding areas that is directly absorbed into the ground, causing it to heat up faster than other ground cover ranges. This could be because of the different values of the surface albedo and land surface temperature on residential urban areas and baresoil. The residential areas in the city are generally painted with light colors which increases the albedo value than the baresoil land. In contrast, asphalt roads, pavements, buildings, concrete and other features that make up the urban surfaces tend to slowly release the heat absorbed. A high albedo means the surface reflects the majority of the radiation that hits it and absorbs the rest. However, black asphalt or roads in the urban areas tend to have high land surface temperature and low albedo value due to its thermal characteristic. Black asphalt or roads have a high tendency to absorb solar radiation. In other words, builtup areas tend to retain heat longer than other classes, such as barren land in the city areas, which does not retain heat for as long. These results are consistent with the findings of [Kant et al., \(2009\)](#) which found that areas with baresoil and builtup areas had higher land surface temperature levels, while other categories, such as water and vegetation, had lower land surface temperature values during the day. The results of this study suggest that the wastelands / barren lands have higher temperatures than residential urban areas.

Considering the relationship between landforms and thermal signatures is the most efficient approach in understanding the effect of different landforms on land surface temperature. Spectral indices are the most widely used and applicable method in large-scale research to measure the urban surface characteristic. Evidence from the past studies shows the precise and significant results in urban surface characteristic computation using spectral indices. To investigate the connection of LST with biophysical variables, indices such as NDVI, NDWI and DBSI were derived from Landsat 8. The NDVI has been used extensively to define the overall vegetation and green area conditions. A higher NDVI shows a higher vegetation likelihood. The DBSI can reveal the builtup and barren land of urban areas. High DBSI values generally signify areas with baresoil while mid-range values signify intensive urban development. Based on reflected near-infrared radiation and visible green light, NDWI enhances the open water features. A higher NDWI shows a higher water body likelihood. The relationship between land surface temperature and urban surface characteristics was examined using the Pearson

correlation coefficient. Lower temperatures in vegetation areas are due to processes like transpiration and evapotranspiration. DBSI values ranged between -0.052 and 0.255 , the DBSI value over baresoil and builtup classes showed a positive correlation with LST. It was found that the baresoil and builtup areas have a noticeable effect on the surface urban heat. Water bodies have a little thermal response and are known to be an efficient absorbent of radiation.

Land Contribution Index (CI) and Landscape index (LI)

To accurately identify the connection between the surface parameters and the trajectory of the land surface temperature in the area under study, a contribution index for each type of land cover was calculated for the summer and winter seasons. The results of the calculated contribution indices of the land use/land cover types show the dominance of the baresoil surface in relation to the impact on the overall land surface temperature regime of the study area. This trend might be explained by the fact that the baresoil land cover type is one of the two groups with a positive net contribution index. Second, for both seasons, this contribution index is greater than all others combined, suggesting that the baresoil region contributes to more surface heating than any other land use/land cover in the study area or has the largest heat generating capability on the surface. Among the four types, vegetation provided maximum heat mitigating impact in the study area. The contribution index value of water remained the same for both the seasons, indicating that temperature variation over water tends to be less variable due to its high thermal capacity. As expected, baresoil and builtup land had high contribution index in summer, which was significantly lower in winter due to lower solar radiation. Apart from baresoil and builtup land, the other types also provided less heat contribution in winter. These observations can be explained by the rainfall season prior to winter season which leads to more vibrant urban green space and therefore more heat sinking.

Model fitting and evaluation

The worst performances were observed by RT models (2×2 and 5×5). However, NN 2×2 , NN 5×5 , SVM 2×2 and SVM 5×5 models performed moderately good with overall RMSE of 0.617°C , 0.594°C , 0.623°C and 0.615°C , respectively. Although the average estimation by all the models is very close to the average LST calculated using the Landsat 8 data, boxplots show that none of the models was capable to predict the extreme values. The comparative results revealed that the K-NN algorithm outperformed the other models. The lowest overall RMSE was calculated at a value of 0.549°C for KNN 5×5 , followed by, KNN 2×2 (0.561°C).

3. Conclusions and Recommendations

3.1 General

This chapter shows the conclusions obtained for the individual objective. Based on the conclusions, recommendations and suggestions have been given.

3.2 Conclusions

1. All the DEMs used in the study have imperfections for the delineation of the small river like Vishwamitri. Moreover, a comparison shows that SRTM 30 m and ASTER 30 m failed to delineate main drainage for the Vishwamitri river. However, Cartosat 30 m DEM exhibited better results. The Cartosat-generated drainage network is much closer to the actual river network followed by the SRTM-derived drainage network. A large number of sinks in ASTER DEM and SRTM DEM around the actual river have considerably contributed to the deviation in ASTER DEM- and SRTM DEM-derived streams from the actual stream. Such error indicates that there are probably residual and artifactual anomalies that most certainly degraded the overall accuracies of ASTER and SRTM DEMs. Moreover, watersheds delineated by ASTER DEM and SRTM DEM could not follow the ridgeline and hence they have encompassed the Dhadhar river in them. It can be concluded that for hydrological studies, the Cartosat DEM should be given first preference followed by the SRTM DEM for the area under study, where the relief class belongs to a flat relief.
2. Principal Component Analysis (PCA) based approach is far superior to the traditional approach for classification. PCA extract the useful spectral information by compressing redundant data embedded in each spectral channel. The overall classification accuracy of MLE classifier was increased from 22% to 41% (19% increase) in the PCA based approach. The overall accuracy RF classifier was increased by 10% reaching 70%, whereas SVM classifier outperformed both the classifiers with 76% overall accuracy (increased by 12%). PCA with Support Vector Machine is able to produce highly accurate land use and land cover classified maps. Support Vector Machine outperformed the Maximum Likelihood Estimation and Random Forest Tree classifiers in both traditional as well as PCA based approach even with a small training dataset. The uncorrelated principal component bands enhanced the classification accuracy as compared to the use of Sentinel-2 original bands. This confirms the feasibility of PCA in remote sensing to extract land use and land cover information and enhance the classification accuracy.
3. The morphometric parameters derived from the Cartosat-1 digital elevation model (30 meters) helped to understand the hydrological behaviour of various sub-watersheds of Vishwamitri watershed. Based on the integration of flood influencing parameters and calculated compound

value, the Sub-watershed I and IV ($C_v= 3.64$) of Vishwamitri watershed have been categorized into high priority, Sub-watershed II ($C_v= 2.91$) and V ($C_v= 2.64$) into moderate priority, and Sub-watershed III ($C_v= 2.18$) into low priority. Morphometric parameters are ideal for providing fundamental data for drawing conclusions that concern the effect of river morphology on the flood situation. In countries like India, high maintenance costs and the requirement for skilled operators make providing gauge stations to each watershed probably expensive. As remote sensing data are widely used in mathematical watershed models to simulate and evaluate the existing and proposed management scenarios, the runoff curve numbers estimated from remotely sensed parameters, such as land use and land cover and soil data, in combination with observed rainfall, predicted runoff and peak flow, may result in high accuracy of hydrological modeling.

4. Suitability map of potential runoff storage zones by integrating the thematic layers of slope derived by topographic position index, LULC, curve number, height above nearest drainage, stream order and topography wetness index using analytic hierarchy process and weighted overlay process within GIS is reliable and accurate. Result shows that 17 % of the study area is optimally suitable, 33.2% of the area is moderately suitable, 33.1 % of the area is marginally suitable and 18.7% of the area is not suitable for water storage zones/structures. Proposed suitability map for potential water storage zones developed by the GIS technique for the study area may be implemented in the future to overcome growing water scarcity due to global/regional climate change. Since the approach and the analysis showed in this research have non-exclusive relevance, they are exceptionally valuable for other parts of the world, especially for developing countries, despite hydrological and agro-climatic variations. This approach is less time-consuming, more precise and can be utilized for identifying potential locations for different interventions for large watersheds. Results will help concerned authorities in the proficient arranging and execution of water-related plans and schemes, improve water shortage, reduce dependability on ground water and ensure sustainable water availability for local and agricultural purposes.
5. Effective and quick response is required during disasters like flooding. Rapid mapping of such events will be beneficial to urban and infrastructure planners, risk managers and disaster responses during extreme and intense rainfall events. The research carried out shows a simple and efficient method for mapping inundation extent with only the C-band of S1A, with coarser geometric resolution and fixed polarizations (VV-VH) by considering the case of Kerala and Assam. Based on the analysis of the obtained results it can be concluded that the the side-looking geometry inherent to conventional SAR sensors leads to the production of radar

shadowing and layover. The backscattering coefficient values become high as the water roughness causes high signal return, decreasing the contrast and making the separation of the land-water covers difficult. Despeckle filters with good noise removal capabilities often tend to degrade the spatial and radiometric resolution of an original data and cause the loss of image details. This may be acceptable for applications involving large scale image interpretation or mapping. However, the retention of the subtle structures of an image is important and, therefore, the performance of speckle noise suppression technique must be balanced with the filter's effectiveness to preserve the fine details. The performance evaluation of de-noising methods in the study showed that Lee filter with 3×3 kernel size provided a good balance in feature preservation as well in despeckling compared to the other filters used in the study. The accuracy assessment of machine learning algorithms for flood classification over Kerala shows that random forest classifier has higher overall classification accuracy (88.80%) than the support vector machine (about 5% higher in VV polarization). However, both the classifiers performed slightly better in VV polarization than VH polarization for Kerala region. For study area Assam, SVM in VH polarization achieved higher overall accuracy (92%) and least performance was observed by RF in VV polarization. It is also concluded that, a single threshold should not be used as large swath of a SAR image suffers from environment heterogeneity caused by wind-roughening and satellite framework parameters.

6. The proposed approach shows the potential for monitoring damages caused by floods, providing basic information that can help local communities manage water-related risk, planning land and water management as well as other flood control programs.

The hydrodynamic-based surface runoff computations in rainfall-runoff simulation at the catchment scale shows the application of the hydrodynamic model HEC-RAS for identifying the inundation areas, in regions with very limited or no ground-based observational data. Ward numbers 2, 5, 6, 8 of Vadodara city were severely affected by the flood and percentage of area inundated in these wards varies from 35.69% to 39.86%. Ward numbers 4, 7, 10, 12 were moderately affected by the flood and percentage of area inundated in these wards varies from 16.34% to 21.92%. Ward numbers 1, 3, 9, 11 were marginally affected by the flood and percentage of area inundated in these wards varies from 0.56% to 3.54%. Moreover, 55.65% of total flood extent are located in the very low hazard class (H1) followed by H4—high hazard class (17.73% of total flood extent), H3—medium hazard class (14.69% of total flood extent), H2—low hazard class (7.26% of total flood extent), H5—extreme hazard class (4.67% of total flood extent). A significant advantage of the given framework is considered to be its ability to produce results using only good quality topographical, rainfall, land use and soil data. In this

way, the technique will yield results for ungauged catchments. The integrated analysis of morphometric, land cover, and topographic analysis for characterising the hydrological behaviour of the Vishwamitri watershed, as shown in this study, may be the sensible alternative until the automated observation network is built in such areas. For validating and calibrating the hydrological simulation models, the availability of the discharge data is crucial. Therefore, the establishment of a network of hydrometeorological and river discharge stations in the basin to facilitate better prediction of the flooding process is of the utmost importance.

7. Spatial distribution of land surface temperature provides critical information for the understanding of local climatic conditions in the cities and can be used as a potential measure to introduce necessary steps to minimize the adverse effects of high land surface temperature. The results indicated the highest land surface temperature was recorded for bare soil while the lowest was recorded for water bodies. Based on research results, the study suggests that a new urban heat mitigation strategy is an important element in the spatial arrangement of impermeable surfaces and green areas as well as water bodies that manage urban heating and cooling. The evaluation of the prediction models shows that the K-NN, NN and SVM models, are the optimum models for predicting the land surface temperature in Vadodara city using neighboring biophysical independent variables relationship with land surface temperature. In addition, it is shown that the K-NN (5×5 observation grid) model exhibits good performance with RMSE of 0.549 °C. The model can help to predict land surface temperature under temporary cloud cover spots, which are present in the data at the time of the acquisition using neighboring biophysical (cloud free) independent variables relationship with land surface temperature.

3.3 Recommendations

1. DEM data with a high spatial resolution must be used. Accurate terrain or morphologically accurate data have a significant effect on geoscientific and hydrological studies such as flood risk prediction, morphometry, 2D hydraulic modelling and so on. Some of these applications include quantitative terrain descriptors derived from DEMs such as slope, aspect, curvature, drainage networks, or watershed delineation to describe shape and topology. Despite the real importance of the applications of DEMs in numerous fields and the technological advances for its creation and availability, aerial photographs or globally available DEMs such as ASTER and SRTM are commonly used, which leads to low accuracy due to the significant effect of inherited anomalies in the DEMs. According to the results analysed in this study, the Cartosat DEM should be given first preference followed by the SRTM DEM for the study area where the relief class belongs to a flat relief. It is also recommended to use DEMs produced by advancement of

current technologies such as light detection and ranging (LiDAR) systems. LiDAR data are much denser sample models of Earth's continuous and irregular surface, should be preferred, if a more detailed and robust analysis is being pursued. It is an efficient technique to provide terrain data with high resolution as compared to other DEM sources. The use of a LiDAR system to generate DEM data has many advantages over other methods. LiDAR data can be collected during the day, night, and even in cloudy conditions. Moreover, it has the ability to penetrate the ground surface in vegetated and urban areas more reliably than either photogrammetry or Interferometric Synthetic Aperture Radar (IfSAR).

2. It is recommended to use principal component analysis for image compression and eliminating noise, redundancy, and irrelevant information which ultimately leads to reduction in the computation costs without compromising the desired variability in the data. Principal component analysis coupled with Support Vector Machine will be appropriate for multispectral as well as for hyperspectral images with small structures or artifacts to detect, or where spectral groups or spectrally related classes predominate, as it minimizes classification errors and make them superior to the parametric classifiers for obtaining effective LULC classification.
3. The cost of implementing a GIS is significant, particularly when the cost of data collection and manipulation is incorporated. The map data and tabular data documenting tracts of land use and cover have been time-consuming and costly to update. When the application area is greater than a few square kilometers, the use of satellite images is justified since defining curve numbers using conventional methods is time-consuming. The determination of the curve number is dependent on the resolution of the satellite, and higher spectral and spatial resolution may provide more accurate estimates. To achieve satisfactory results, further research is needed to be carried out with finer resolution.
4. In the sense of near real-time mapping, it is important to collect data as soon as a flood event occurs. The temporal fusion of SAR and optical data will reduce the time between the flood and data acquisition. Furthermore, the spatial fusion of SAR and optical data may aid in the detection of inundated areas in steep slope terrains that are difficult to detect using SAR data due to radar shadowing and foreshortening. It is recommended to use VH and VV polarization for flood area mapping application due to the reduced nature of scattering and speckles in absence of HH polarization. SAR data has a number of drawbacks that must be considered during the data collection process, such as the inability to record flooding in urban areas due to the corner reflection concept, double-bounce effect, noise, and increased measurement uncertainty due to speckle. Such a radar response is insufficient for mapping the real flooded areas of urban areas. As a result, in the context of a real-time disaster situation, flood area

mapping of urban areas is a difficult job and should be typically handled by domain experts using a LiDAR height map of the urban area aided with hydraulic modelling. A comprehensive evaluation of further Sentinel-1 scenes is expected in the future, including a thorough study of the performance of VV and VH polarization in various environments and wind conditions. Since Sentinel-1 imagery is collected in a systematic manner, time-series analysis may help us enhance the robustness of the flood mapping workflow provided.

5. Mitigation steps should be implemented in upper tributary streams, such as an early flood warning system, introduction of water storage areas (check dams), levees/embankments, flood walls, flood gates, strategic agriculture, the creation of flood risk maps, the prevention of further growth in flood-prone areas, and the adaptation of advanced flood forecasting techniques.
6. In order to mitigate floods, it is proposed that there is a significant need to create a flood spill channel that can take up one-third of the total flow of the Vishwamitri River. Moreover, to prevent floods in the downstream agricultural areas and settlements, additional reservoir must be created in Sub-watershed I. Along with this, mitigation measures such as check dams, nala bunds, gully plug, bundhis (local name in India), percolation tanks etc. can be constructed in a planned and systematic manner in Sub-watershed I, II and IV to create water buffer within the catchment, which will help reducing vulnerability to seasonal variations in rainfall.
7. Vishwamitri River discharges have to be measured accurately with uniformity in time of observations. For this purpose automated observation network of gauging stations would need to be established in each sub-watershed with current meter observations, where the river section is relatively straight and uniform, free of obstructions and vegetation, with no progressive tendency to scour or accrete, and free of the backwater effect of tributaries, downstream structures (dams, bridges). The flow should be contained within defined boundaries. Gauge site should be sensitive to the extent that a significant change in discharge, even for the lowest discharges, should be accompanied by a significant change in stage. Gauges will have to be established with gauge levels conforming to G.T.S. (Great Trigonometrical Survey) benchmark so that they are connected to common datum.
8. To overcome growing water scarcity due to global/regional climate change, water storage structures must be made on potential water storage zones as shown in the study. More investments in infrastructure development (i.e., dams and water supply pipe networks) would help future population cope with the growing water demand as an uneven distribution of precipitation in time is expected due to climate change. Ponds are suitable for small flat areas with slopes 5%, 0.15 % of study area belongs to middle slope, nala bunds are suitable on

moderate slopes of 5–10%, 12.49 % study area belongs to upper slope, terracing is suitable for steeper slopes of 5–30%. Ridges and upper slope together forms 30.79 % of the study area, they indicate least potential for rainwater harvesting because higher sloping land is inappropriate for constructing water storage structures. Valley and lower slope together constitutes for 33.58 % of the study area, small dams or check dams like structures are preferable on such sites.

9. Rising global temperatures pose a growing challenge to safe and healthy living conditions. Because of the materials used to construct houses, streets, and infrastructure, these environmental changes have had a particularly negative impact on cities. Increasing the albedo of roofs appears to be an effective approach to reduce the temperature rises caused by urban heat island and also the least-cost alternative compared with green roofs and urban forestry. It is therefore recommended that the Vadodara city employ heat mitigation strategies such as the use of high albedo urban materials, reflective pavements, increasing the area of vegetated land in the city, green roofs, addition of large urban bodies of water, etc.

7. References

1. Abuzied, S., Yuan, M., Ibrahim, S., Kaiser, M., & Saleem, T. (2016). Geospatial risk assessment of flash floods in Nuweiba area, Egypt. *Journal of Arid Environments*, 133, 54-72.
2. Adegoke, C. W., & Sojobi, A. O. (2015). Climate change impact on infrastructure in Osogbo metropolis, south-west Nigeria. *Journal of Emerging Trends in Engineering and Applied Sciences*, 6(3), 156-165.
3. Ågren, A. M., Lidberg, W., Strömberg, M., Ogilvie, J., & Arp, P. A. (2014). Evaluating digital terrain indices for soil wetness mapping—a Swedish case study. *Hydrology and Earth System Sciences*, 18(9), 3623-3634.
4. Ahmed, B., Kamruzzaman, M. D., Zhu, X., Rahman, M., & Choi, K. (2013). Simulating land cover changes and their impacts on land surface temperature in Dhaka, Bangladesh. *Remote Sensing*, 5(11), 5969-5998.
5. Ahmed, S. A., Chandrashekarappa, K. N., Raj, S. K., Nischitha, V., & Kavitha, G. (2010). Evaluation of morphometric parameters derived from ASTER and SRTM DEM—a study on Bandihole sub-watershed basin in Karnataka. *Journal of the Indian society of remote sensing*, 38(2), 227-238.
6. Akinsanola, A. A., & Ogunjobi, K. O. (2014). Analysis of rainfall and temperature variability over Nigeria. *Global Journal of Human Social Sciences: Geography & Environmental GeoSciences*, 14(3), 1-18.
7. Al-Adamat, R. (2008). GIS as a decision support system for siting water harvesting ponds in the Basalt Aquifer/NE Jordan. *Journal of Environmental Assessment Policy and Management*, 10(02), 189-206.
8. Altaf, F., Meraj, G., & Romshoo, S. A. (2013). Morphometric analysis to infer hydrological behaviour of Lidder watershed, Western Himalaya, India. *Geography Journal*, 2013.
9. Amani, M., Salehi, B., Mahdavi, S., Granger, J., & Brisco, B. (2017). Wetland classification in Newfoundland and Labrador using multi-source SAR and optical data integration. *GIScience & Remote Sensing*, 54(6), 779-796.
10. Ammar, A., Riksen, M., Ouessar, M., & Ritsema, C. (2016). Identification of suitable sites for rainwater harvesting structures in arid and semi-arid regions: A review. *International Soil and Water Conservation Research*, 4(2), 108-120.
11. Ammar, A., Riksen, M., Ouessar, M., & Ritsema, C. (2016). Identification of suitable sites for rainwater harvesting structures in arid and semi-arid regions: A review. *International Soil and Water Conservation Research*, 4(2), 108-120.
12. Asselman, N., Maat, J. T., Wit, A. D., Verhoeven, G., Frazão, S., Velickovic, M., & Bates, P. (2009). Flood inundation modelling. *Executive summary, Report*, (T08-08), 01.
13. Avdan, U., & Jovanovska, G. (2016). Algorithm for automated mapping of land surface temperature using LANDSAT 8 satellite data. *Journal of sensors*, 2016.
14. Awange, J. L., & Kiema, J. B. K. (2013). Optical Remote Sensing. In *Environmental Geoinformatics* (pp. 119-132). Springer, Berlin, Heidelberg.

15. Bannari, A., Ghadeer, A., El-Battay, A., Hameed, N. A., & Rouai, M. (2017). Detection of areas associated with flash floods and erosion caused by rainfall storm using topographic attributes, hydrologic indices, and GIS. In *Global Changes and Natural Disaster Management: Geo-information Technologies* (pp. 155-174). Springer, Cham.
16. Barsi, J. A., Schott, J. R., Hook, S. J., Raqueno, N. G., Markham, B. L., & Radocinski, R. G. (2014). Landsat-8 thermal infrared sensor (TIRS) vicarious radiometric calibration. *Remote Sensing*, *6*(11), 11607-11626.
17. Belgiu, M., & Csillik, O. (2018). Sentinel-2 cropland mapping using pixel-based and object-based time-weighted dynamic time warping analysis. *Remote sensing of environment*, *204*, 509-523.
18. Beven, K. J., & Kirkby, M. J. (1979). A physically based, variable contributing area model of basin hydrology/Un modèle à base physique de zone d'appel variable de l'hydrologie du bassin versant. *Hydrological Sciences Journal*, *24*(1), 43-69.
19. Bhat, M. S., Alam, A., Ahmad, S., Farooq, H., & Ahmad, B. (2019). Flood hazard assessment of upper Jhelum basin using morphometric parameters. *Environmental Earth Sciences*, *78*(2), 54.
20. Bhatt, S., & Ahmed, S. A. (2014). Morphometric analysis to determine floods in the Upper Krishna basin using Cartosat DEM. *Geocarto international*, *29*(8), 878-894.
21. Bisht, S., Chaudhry, S., Sharma, S., & Soni, S. (2018). Assessment of flash flood vulnerability zonation through Geospatial technique in high altitude Himalayan watershed, Himachal Pradesh India. *Remote Sensing Applications: Society and Environment*, *12*, 35-47.
22. Bitterman, P., Tate, E., Van Meter, K. J., & Basu, N. B. (2016). Water security and rainwater harvesting: A conceptual framework and candidate indicators. *Applied Geography*, *76*, 75-84.
23. Bjelanovic, I. (2016). Predicting forest productivity using Wet Areas Mapping and other remote sensed environmental data.
24. Breiman, L. (2001). Random forests. *Machine learning*, *45*(1), 5-32.
25. Bruniquel, J., & Lopes, A. (1997). Multi-variate optimal speckle reduction in SAR imagery. *International Journal of Remote Sensing*, *18*(3), 603-627. <https://doi.org/10.1080/014311697218962>
26. Burnside, N., Smith, R., & Waite, S. (2002). Habitat suitability modelling for calcareous grassland restoration on the South Downs, United Kingdom. *Journal of Environmental Management*, *65*(2), 209e221.
27. Burrough, P. A., van Gaans, P. F., & MacMillan, R. A. (2000). High-resolution landform classification using fuzzy k-means. *Fuzzy sets and systems*, *113*(1), 37-52.
28. Campbell, J. B., & Wynne, R. H. (2011). *Introduction to remote sensing*. Guilford Press.
29. Candade, N., & Dixon, B. (2004, May). Multispectral classification of Landsat images: a comparison of support vector machine and neural network classifiers. In *ASPRS Annual Conference Proceedings, Denver, Colorado*.
30. Central Water Commission. (2018). *Kerala Floods August 2018*. Retrieved from <https://reliefweb.int/sites/reliefweb.int/files/resources/Rev-0.pdf>
31. Chaplot, V. (2014). Impact of spatial input data resolution on hydrological and erosion modeling: Recommendations from a global assessment. *Physics and Chemistry of the Earth, Parts A/B/C*, *67*, 23-35.

32. Chen, L., Fu, B., & Zhao, W. (2008). Source-sink landscape theory and its ecological significance. *Frontiers of Biology in China*, 3(2), 131-136.
33. Chen, N. (2020). Mapping mangrove in Dongzhaigang, China using Sentinel-2 imagery. *Journal of Applied Remote Sensing*, 14(1), 014508.
34. Chen, X., & Zhang, Y. (2017). Impacts of urban surface characteristics on spatiotemporal pattern of land surface temperature in Kunming of China. *Sustainable Cities and Society*, 32, 87-99.
35. Cheng, G., Han, J., Guo, L., Liu, Z., Bu, S., & Ren, J. (2015). Effective and efficient midlevel visual elements-oriented land-use classification using VHR remote sensing images. *IEEE Transactions on Geoscience and Remote Sensing*, 53(8), 4238-4249.
36. Chunming, H., Huadong, G., Yun, S., & Jingjuan, L. (2005, July). Detection of the flood boundary in SAR image using texture. In *Proceedings. 2005 IEEE International Geoscience and Remote Sensing Symposium, 2005. IGARSS'05.* (Vol. 5, pp. 3697-3699). IEEE.
37. Cigdem, A., & Ozden, C. (2018). Predicting the severity of motor vehicle accident injuries in Adana-turkey using machine learning methods and detailed meteorological data. *International Journal of Intelligent Systems and Applications in Engineering*, 6(1), 72-79.
38. Congalton, R. G. (2001). Accuracy assessment and validation of remotely sensed and other spatial information. *International Journal of Wildland Fire*, 10(4), 321-328.
39. Costabile, P., Costanzo, C., Ferraro, D., Macchione, F., & Petaccia, G. (2020). Performances of the new HEC-RAS version 5 for 2-D hydrodynamic-based rainfall-runoff simulations at basin scale: Comparison with a state-of-the art model. *Water*, 12(9), 2326.
40. Costabile, P., Macchione, F., Natale, L., & Petaccia, G. (2015). Flood mapping using LIDAR DEM. Limitations of the 1-D modeling highlighted by the 2-D approach. *Natural Hazards*, 77(1), 181-204.
41. Cunningham, P., & Delany, S. J. (2020). k-Nearest Neighbour Classifiers---. *arXiv preprint arXiv:2004.04523*.
42. Dasallas, L., & Lee, S. (2019). Topographical Analysis of the 2013 Typhoon Haiyan Storm Surge Flooding by Combining the JMA Storm Surge Model and the FLO-2D Flood Inundation Model. *Water*, 11(1), 144.
43. de Leeuw, M. R., & de Carvalho, L. M. T. (2009). Performance evaluation of several adaptive speckle filters for SAR imaging. *Anais XIV Simpósio Brasileiro de Sensoriamento Remoto*, 7299-7305.
44. De Pauw, E. (2018). Integrating expert knowledge in GIS to locate biophysical potential for water harvesting: methodology and a case study for Syria.
45. De Winnaar, G., Jewitt, G. P. W., & Horan, M. (2007). A GIS-based approach for identifying potential runoff harvesting sites in the Thukela River basin, South Africa. *Physics and Chemistry of the Earth, Parts A/B/C*, 32(15-18), 1058-1067.
46. Deng, G. O. (1998). Principal component analysis of stacked multi-temporal images for the monitoring of rapid urban expansion in the Pearl River Delta. *International Journal of Remote Sensing*, 19(8), 1501-1518. <https://doi.org/10.1080/014311698215315>

47. Deumlich, D., Schmidt, R., & Sommer, M. (2010). A multiscale soil–landform relationship in the glacial-drift area based on digital terrain analysis and soil attributes. *Journal of Plant Nutrition and Soil Science*, 173(6), 843-851.
48. Dilts, T.E., 2015. Topography Tools for ArcGIS 10.1. Available at: <http://www.arcgis.com/home/item.html?id=b13b3b40fa3c43d4a23a1a09c5fe96b9>.
49. Drucker, H., Burges, C. J., Kaufman, L., Smola, A. J., & Vapnik, V. (1997). Support vector regression machines. In *Advances in neural information processing systems* (pp. 155-161).
50. Dumitru, C. O., Cui, S., Faur, D., & Datcu, M. (2014). Data analytics for rapid mapping: Case study of a flooding event in Germany and the tsunami in Japan using very high resolution SAR images. *IEEE Journal of Selected Topics in Applied Earth Observations and Remote Sensing*, 8(1), 114-129.
51. Durand, J. M., Gimonet, B. J., & Perbos, J. R. (1987). SAR data filtering for classification. *IEEE Transactions on Geoscience and Remote Sensing*, (5), 629-637.
52. Durga Rao, K. H. V., & Bhaumik, M. K. (2003). Spatial expert support system in selecting suitable sites for water harvesting structures—a case study of song watershed, Uttaranchal, India. *Geocarto International*, 18(4), 43-50.
53. Durga Rao, K. H. V., & Bhaumik, M. K. (2003). Spatial expert support system in selecting suitable sites for water harvesting structures—a case study of song watershed, Uttaranchal, India. *Geocarto International*, 18(4), 43-50.
54. Elkhrachy, I. (2015). Flash flood hazard mapping using satellite images and GIS tools: a case study of Najran City, Kingdom of Saudi Arabia (KSA). *The Egyptian Journal of Remote Sensing and Space Science*, 18(2), 261-278.
55. Eze, E. B., & Efiog, J. (2010). Morphometric parameters of the Calabar river basin: Implication for hydrologic processes. *Journal of Geography and Geology*, 2(1), 18.
56. FAO, 2003. Land and Water Digital Media Series, 26. Training Course on RWH (CDROM). Planning of Water Harvesting Schemes, Unit 22. Food and Agriculture Organization of the United Nations, Rome, FAO.
57. Fassoni-Andrade, A. C., Fan, F. M., Collischonn, W., Fassoni, A. C., & Paiva, R. C. D. D. (2018). Comparison of numerical schemes of river flood routing with an inertial approximation of the Saint Venant equations. *RBRH*, 23.
58. Feldman, A. D. (2000). Hydrologic modeling system HEC-HMS: technical reference manual. US Army Corps of Engineers, Hydrologic Engineering Center.
59. Firozjarei, M. K., Alavipanah, S. K., Liu, H., Sedighi, A., Mijani, N., Kiavarz, M., & Weng, Q. (2019). A PCA–OLS model for assessing the impact of surface biophysical parameters on land surface temperature variations. *Remote Sensing*, 11(18), 2094.
60. Foody, G. M., & Mathur, A. (2004). Toward intelligent training of supervised image classifications: directing training data acquisition for SVM classification. *Remote Sensing of Environment*, 93(1-2), 107-117.
61. Francés, A. P., & Lubczynski, M. W. (2011). Topsoil thickness prediction at the catchment scale by integration of invasive sampling, surface geophysics, remote sensing and statistical modeling. *Journal of hydrology*, 405(1-2), 31-47.
62. Frost, V. S., Stiles, J. A., Shanmugan, K. S., & Holtzman, J. C. (1982). A model for radar images and its application to adaptive digital filtering of multiplicative noise. *IEEE Transactions on pattern analysis and machine intelligence*, (2), 157-166.

63. Fu, B., Wang, Y., Campbell, A., Li, Y., Zhang, B., Yin, S., ... & Jin, X. (2017). Comparison of object-based and pixel-based Random Forest algorithm for wetland vegetation mapping using high spatial resolution GF-1 and SAR data. *Ecological indicators*, 73, 105-117.
64. GALLANT, J. C. (2000). Primary topographic attributes. *Terrain analysis-principles and application*, 51-86.
65. Ghani, M. W., Arshad, M., Shabbir, A., Mehmood, N., & Ahmad, I. (2013). Investigation of potential water harvesting sites at Potohar using modeling approach. *Pakistan Journal of Agricultural Sciences*, 50(4).
66. Ghimire, B., Rogan, J., Galiano, V. R., Panday, P., & Neeti, N. (2012). An evaluation of bagging, boosting, and random forests for land-cover classification in Cape Cod, Massachusetts, USA. *GIScience & Remote Sensing*, 49(5), 623-643.
67. Gioti, E., Riga, C., Kalogeropoulos, K., & Chalkias, C. (2013). A GIS-based flash flood runoff model using high resolution DEM and meteorological data. *EARSeL eProceedings*, 12(1), 33-43.
68. Gislason, P. O., Benediktsson, J. A., & Sveinsson, J. R. (2006). Random forests for land cover classification. *Pattern recognition letters*, 27(4), 294-300.
69. Gitas, I. Z., Polychronaki, A., Katagis, T., & Mallinis, G. (2008). Contribution of remote sensing to disaster management activities: A case study of the large fires in the Peloponnese, Greece. *International journal of remote sensing*, 29(6), 1847-1853.
70. Goodman, J. W. (1976). Some fundamental properties of speckle. *JOSA*, 66(11), 1145-1150.
71. Guth, P. L. (2010, November). Geomorphometric comparison of ASTER GDEM and SRTM. In *A special joint symposium of ISPRS Technical Commission IV & AutoCarto in conjunction with ASPRS/CaGIS*.
72. Haashemi, S., Weng, Q., Darvishi, A., & Alavipanah, S. K. (2016). Seasonal variations of the surface urban heat island in a semi-arid city. *Remote Sensing*, 8(4), 352.
73. Hamdani, N., & Baali, A. (2019). Height Above Nearest Drainage (HAND) model coupled with lineament mapping for delineating groundwater potential areas (GPA). *Groundwater for Sustainable Development*, 9, 100256.
74. Hameed, H. M., Faqe, G. R., & Rasul, A. (2019). Effects of Land Cover Change on Surface Runoff Using GIS and Remote Sensing. *Environmental Remote Sensing and GIS in Iraq*, 205.
75. Han, J., Zhang, D., Cheng, G., Guo, L., & Ren, J. (2014). Object detection in optical remote sensing images based on weakly supervised learning and high-level feature learning. *IEEE Transactions on Geoscience and Remote Sensing*, 53(6), 3325-3337.
76. Handayani, H. H., Murayama, Y., Ranagalage, M., Liu, F., & Dissanayake, D. M. S. L. B. (2018). Geospatial analysis of horizontal and vertical urban expansion using multi-spatial resolution data: A case study of Surabaya, Indonesia. *Remote Sensing*, 10(10), 1599.
77. Hassan, Z., Shabbir, R., Ahmad, S. S., Malik, A. H., Aziz, N., Butt, A., & Erum, S. (2016). Dynamics of land use and land cover change (LULCC) using geospatial techniques: a case study of Islamabad Pakistan. *SpringerPlus*, 5(1), 1-11.
78. Hengl, T., & Reuter, H. I. (Eds.). (2008). *Geomorphometry: concepts, software, applications*. Newnes.

79. Hojati, M., & Mokarram, M. (2016). Determination of a topographic wetness index using high resolution digital elevation models. *European Journal of Geography*, 7(4), 41-52.
80. Horton, R. E. (1945). Erosional development of streams and their drainage basins; hydrophysical approach to quantitative morphology. *Geological society of America bulletin*, 56(3), 275-370.
81. Huang, C., Davis, L. S., & Townshend, J. R. G. (2002). An assessment of support vector machines for land cover classification. *International Journal of remote sensing*, 23(4), 725-749.
82. Huang, Q., Huang, J., Yang, X., Fang, C., & Liang, Y. (2019). Quantifying the seasonal contribution of coupling urban land use types on Urban Heat Island using Land Contribution Index: A case study in Wuhan, China. *Sustainable Cities and Society*, 44, 666-675.
83. IBM. (2015). SPSS Modeler 17 Applications guide. <ftp://public.dhe.ibm.com/software/analytics/spss/documentation/modeler/17.0/en/ModelerApplications.pdf>
84. Illés, G., Kovács, G., & Heil, B. (2011). Comparing and evaluating digital soil mapping methods in a Hungarian forest reserve. *Canadian Journal of Soil Science*, 91(4), 615-626.
85. Immitzer, M., Atzberger, C., & Koukal, T. (2012). Tree species classification with random forest using very high spatial resolution 8-band WorldView-2 satellite data. *Remote sensing*, 4(9), 2661-2693.
86. IMSD, (1995). Integrated Mission for Sustainable Development technical guidelines, National Remote Sensing Agency, Department of Space, Govt. of India.
87. India Meteorological Department. (2018). *Rainfall over Kerala during Monsoon Season-2018 and forecast for next 5 days*. Retrieved from [https://www.imdtvm.gov.in/images/rainfall over kerala during monsoon season-2018 and forecast for next 5 days.pdf](https://www.imdtvm.gov.in/images/rainfall%20over%20kerala%20during%20monsoon%20season-2018%20and%20forecast%20for%20next%205%20days.pdf)
88. Iosub, M., Minea, I., Chelariu, O. E., & Ursu, A. (2020). Assessment of flash flood susceptibility potential in Moldavian Plain (Romania). *Journal of Flood Risk Management*, 13(4), e12588.
89. Iwahashi, J., & Pike, R. J. (2007). Automated classifications of topography from DEMs by an unsupervised nested-means algorithm and a three-part geometric signature. *Geomorphology*, 86(3-4), 409-440.
90. Janssen, L. L., & Vanderwel, F. J. (1994). Accuracy assessment of satellite derived land-cover data: a review. *Photogrammetric engineering and remote sensing;(United States)*, 60(4).
91. Jarihani, A. A., Callow, J. N., McVicar, T. R., Van Niel, T. G., & Larsen, J. R. (2015). Satellite-derived Digital Elevation Model (DEM) selection, preparation and correction for hydrodynamic modelling in large, low-gradient and data-sparse catchments. *Journal of Hydrology*, 524, 489-506.
92. Javed, F., Chan, G. S., Savkin, A. V., Middleton, P. M., Malouf, P., Steel, E., ... & Lovell, N. H. (2009, September). RBF kernel based support vector regression to estimate the blood volume and heart rate responses during hemodialysis. In *2009 Annual International Conference of the IEEE Engineering in Medicine and Biology Society* (pp. 4352-4355). IEEE.

93. Jenness, J. (2006). Topographic Position Index (tpi_jen.avx) extension for ArcView 3.x, v.1.3a. Retrieved from <http://www.jennessent.com/arcview/tpi.htm>.
94. Jenson, S. K., & Domingue, J. O. (1988). Extracting topographic structure from digital elevation data for geographic information system analysis. *Photogrammetric engineering and remote sensing*, 54(11), 1593-1600.
95. Jha, M. K., Chowdary, V. M., Kulkarni, Y., & Mal, B. C. (2014). Rainwater harvesting planning using geospatial techniques and multicriteria decision analysis. *Resources, Conservation and Recycling*, 83, 96-111.
96. Käfer, P. S., Rolim, S. B. A., Iglesias, M. L., da Rocha, N. S., & Diaz, L. R. (2019). Land surface temperature retrieval by LANDSAT 8 thermal band: applications of laboratory and field measurements. *IEEE Journal of Selected Topics in Applied Earth Observations and Remote Sensing*, 12(7), 2332-2341.
97. Kahinda, J. Mwenge, E. S. B. Lillie, A. E. Taigbenu, M. Taute, and R. J. Boroto. "Developing suitability maps for rainwater harvesting in South Africa." *Physics and Chemistry of the Earth, Parts A/B/C* 33, no. 8-13 (2008): 788-799.
98. Kant, Y., Bharath, B. D., Mallick, J., Atzberger, C., & Kerle, N. (2009). Satellite-based analysis of the role of land use/land cover and vegetation density on surface temperature regime of Delhi, India. *Journal of the Indian Society of Remote Sensing*, 37(2), 201-214.
99. Karimi, H., & Zeinivand, H. (2021). Integrating runoff map of a spatially distributed model and thematic layers for identifying potential rainwater harvesting suitability sites using GIS techniques. *Geocarto International*, 36(3), 320-339.
100. Karmokar, S., & De, M. (2020). Flash flood risk assessment for drainage basins in the Himalayan foreland of Jalpaiguri and Darjeeling Districts, West Bengal. *Modeling Earth Systems and Environment*, 6, 2263-2289.
101. Khatami, R., Mountrakis, G., & Stehman, S. V. (2016). A meta-analysis of remote sensing research on supervised pixel-based land-cover image classification processes: General guidelines for practitioners and future research. *Remote Sensing of Environment*, 177, 89-100.
102. Krois, J., & Schulte, A. (2014). GIS-based multi-criteria evaluation to identify potential sites for soil and water conservation techniques in the Ronquillo watershed, northern Peru. *Applied Geography*, 51, 131-142.
103. Kumar, T., & Jhariya, D. C. (2017). Identification of rainwater harvesting sites using SCS-CN methodology, remote sensing and Geographical Information System techniques. *Geocarto International*, 32(12), 1367-1388.
104. Lama, S., & Maiti, R. (2019). Morphometric Analysis of Chel River Basin, West Bengal, India, using Geographic Information System. *Earth Science India*, 12(1).
105. Lee, J. S. (1981). Speckle analysis and smoothing of synthetic aperture radar images. *Computer graphics and image processing*, 17(1), 24-32.
106. Lee, J. S., & Pottier, E. (2017). *Polarimetric radar imaging: from basics to applications*. CRC press.
107. Lee, J. S., Jurkevich, L., Dewaele, P., Wambacq, P., & Oosterlinck, A. (1994). Speckle filtering of synthetic aperture radar images: A review. *Remote sensing reviews*, 8(4), 313-340.

108. Lesschen, J. P., Kok, K., Verburg, P. H., & Cammeraat, L. H. (2007). Identification of vulnerable areas for gully erosion under different scenarios of land abandonment in Southeast Spain. *Catena*, *71*(1), 110-121.
109. Li, J. (2021). Fundamentals of Satellite Remote Sensing Technology. In *Satellite Remote Sensing Technologies* (pp. 1-26). Springer, Singapore.
110. Li, J., & Wong, D. W. S. (2010). Computers, environment and urban systems effects of DEM sources on hydrologic applications. *Comput Environ Urban Syst*, *34*(3), 251-261.
111. Liu, H., Bu, R., Liu, J., Leng, W., Hu, Y., Yang, L., & Liu, H. (2011). Predicting the wetland distributions under climate warming in the Great Xing'an Mountains, northeastern China. *Ecological research*, *26*(3), 605-613.
112. Liu, M., Hu, Y., Chang, Y., He, X., & Zhang, W. (2009). Land use and land cover change analysis and prediction in the upper reaches of the Minjiang River, China. *Environmental management*, *43*(5), 899-907.
113. Lopes, A., Nezry, E., Touzi, R., & Laur, H. (1990, May). Maximum a posteriori speckle filtering and first order texture models in SAR images. In *10th annual international symposium on geoscience and remote sensing* (pp. 2409-2412). Ieee.
114. Loritz, R., Kleidon, A., Jackisch, C., Westhoff, M., Ehret, U., Gupta, H., & Zehe, E. (2019). A topographic index explaining hydrological similarity by accounting for the joint controls of runoff formation. *Hydrology and Earth System Sciences*, *23*(9), 3807-3821.
115. Lu, D., Mausel, P., Brondizio, E., & Moran, E. (2004). Change detection techniques. *International journal of remote sensing*, *25*(12), 2365-2401.
116. Ma, Y., Kuang, Y., & Huang, N. (2010). Coupling urbanization analyses for studying urban thermal environment and its interplay with biophysical parameters based on TM/ETM+ imagery. *International Journal of Applied Earth Observation and Geoinformation*, *12*(2), 110-118.
117. Magesh, N. S., & Chandrasekar, N. (2014). GIS model-based morphometric evaluation of Tamiraparani subbasin, Tirunelveli district, Tamil Nadu, India. *Arabian Journal of Geosciences*, *7*(1), 131-141.
118. Mahdianpari, M., Salehi, B., Mohammadimanesh, F., & Brisco, B. (2017). An assessment of simulated compact polarimetric SAR data for wetland classification using random forest algorithm. *Canadian Journal of Remote Sensing*, *43*(5), 468-484.
119. Mahmood, S., & Rahman, A. U. (2019). Flash flood susceptibility modeling using geomorphometric and hydrological approaches in Panjkora Basin, Eastern Hindu Kush, Pakistan. *Environmental earth sciences*, *78*(1), 43.
120. Mahmoud, S. H., & Alazba, A. A. (2015). The potential of in situ rainwater harvesting in arid regions: developing a methodology to identify suitable areas using GIS-based decision support system. *Arabian Journal of Geosciences*, *8*(7), 5167-5179.
121. Malczewski, J., 1999. GIS and Multicriteria Decision Analysis. John Wiley & Sons, Inc.. 392 pp.
122. Malik, S., & Pal, S. C. (2020). Application of 2D numerical simulation for rating curve development and inundation area mapping: a case study of monsoon dominated Dwarkeswar River. *International Journal of River Basin Management*, 1-11.
123. Mallick, J., Kant, Y., & Bharath, B. D. (2008). Estimation of land surface temperature over Delhi using Landsat-7 ETM+. *J. Ind. Geophys. Union*, *12*(3), 131-140.

124. Manandhar, R., Odeh, I. O., & Ancev, T. (2009). Improving the accuracy of land use and land cover classification of Landsat data using post-classification enhancement. *Remote Sensing*, 1(3), 330-344.
125. Markose, V. J., & Jayappa, K. S. (2011). Hypsometric analysis of Kali River Basin, Karnataka, India, using geographic information system. *Geocarto International*, 26(7), 553-568.
126. Martz, L. W., & Garbrecht, J. (1998). The treatment of flat areas and depressions in automated drainage analysis of raster digital elevation models. *Hydrological processes*, 12(6), 843-855.
127. Martz, L. W., & Garbrecht, J. (1999). An outlet breaching algorithm for the treatment of closed depressions in a raster DEM. *Computers & Geosciences*, 25(7), 835-844.
128. Masoud, M. H. (2016). Geoinformatics application for assessing the morphometric characteristics' effect on hydrological response at watershed (case study of Wadi Qanunah, Saudi Arabia). *Arabian Journal of Geosciences*, 9(4), 1-22.
129. Massetti, A., & Gil, A. (2020). Mapping and assessing land cover/land use and aboveground carbon stocks rapid changes in small oceanic islands' terrestrial ecosystems: A case study of Madeira Island, Portugal (2009–2011). *Remote Sensing of Environment*, 239, 111625.
130. Mati, B., De Bock, T., Malesu, M., Khaka, E., Oduor, A., Meshack, M., & Oduor, V. (2006). Mapping the potential of rainwater harvesting technologies in Africa. *A GIS overview on development domains for the continent and ten selected countries. Technical Manual*, 6, 126.
131. Mcfeeters, S.K., 1996. The use of the Normalized Difference Water Index (NDWI) in the delineation of open water features. *Int. J. Remote Sens.* <https://doi.org/10.1080/01431169608948714>.
132. McGarigal, K., Tagil, S., & Cushman, S. A. (2009). Surface metrics: an alternative to patch metrics for the quantification of landscape structure. *Landscape ecology*, 24(3), 433-450.
133. McKee, T. B., Doesken, N. J., & Kleist, J. (1993, January). The relationship of drought frequency and duration to time scales.
134. Mesh type tradeoffs in 2D hydrodynamic modeling of flooding with a Godunov-based flow solver.
135. Min, M., Zhao, H., & Miao, C. (2018). Spatio-temporal evolution analysis of the urban heat island: A case study of Zhengzhou City, China. *Sustainability*, 10(6), 1992.
136. Moges, G., & Bhole, V. (2015). Morphometric characteristics and the relation of stream orders to hydraulic parameters of river Goro: An Ephemeral River in Dire-Dawa, Ethiopia. *Universal Journal of geoscience*, 3(1), 13-27.
137. Mou, H., & Wang, H. (1999). 1 Division Study of Rainwater Utilization in China. Conference, Brazil.
138. Nag, S. K. (1998). Morphometric analysis using remote sensing techniques in the Chaka sub-basin, Purulia district, West Bengal. *Journal of the Indian society of remote sensing*, 26(1-2), 69-76.
139. Nikolakopoulos, K. G., Kamaratakis, E. K., & Chrysoulakis, N. (2006). SRTM vs ASTER elevation products. Comparison for two regions in Crete, Greece. *International Journal of remote sensing*, 27(21), 4819-4838.

140. Nirupama, N., & Simonovic, S. P. (2007). Increase of flood risk due to urbanisation: A Canadian example. *Natural Hazards*, 40(1), 25.
141. Nobre, A. D., Cuartas, L. A., Hodnett, M., Rennó, C. D., Rodrigues, G., Silveira, A., Waterloo, M. & Saleska, S. (2011). Height Above the Nearest Drainage—a hydrologically relevant new terrain model. *Journal of Hydrology*, 404(1-2), 13-29.
142. Ok, A. O., Akar, O., & Gungor, O. (2012). Evaluation of random forest method for agricultural crop classification. *European Journal of Remote Sensing*, 45(1), 421-432.
143. Omran, A., Dietrich, S., Abouelmagd, A., & Michael, M. (2016). New ArcGIS tools developed for stream network extraction and basin delineations using Python and java script. *Computers & Geosciences*, 94, 140-149.
144. Ongdas, N., Akiyanova, F., Karakulov, Y., Muratbayeva, A., & Zinabdin, N. (2020). Application of HEC-RAS (2D) for flood hazard maps generation for Yesil (Ishim) river in Kazakhstan. *Water*, 12(10), 2672.
145. Oommen, T., Misra, D., Twarakavi, N. K., Prakash, A., Sahoo, B., & Bandopadhyay, S. (2008). An objective analysis of support vector machine based classification for remote sensing. *Mathematical geosciences*, 40(4), 409-424.
146. Ozdemir, H., & Bird, D. (2009). Evaluation of morphometric parameters of drainage networks derived from topographic maps and DEM in point of floods. *Environmental geology*, 56(7), 1405-1415.
147. Ozesmi, S. L., & Bauer, M. E. (2002). Satellite remote sensing of wetlands. *Wetlands ecology and management*, 10(5), 381-402.
148. Pal, M., & Mather, P. M. (2005). Support vector machines for classification in remote sensing. *International journal of remote sensing*, 26(5), 1007-1011.
149. Pande, C. B., & Moharir, K. (2017). GIS based quantitative morphometric analysis and its consequences: a case study from Shanur River Basin, Maharashtra India. *Applied Water Science*, 7(2), 861-871.
150. Parastatidis, D., Mitraka, Z., Chrysoulakis, N., & Abrams, M. (2017). Online global land surface temperature estimation from Landsat. *Remote sensing*, 9(12), 1208.
151. Patterson, J. J. (2008). Late Holocene land use in the Nutzotin Mountains: lithic scatters, viewsheds, and resource distribution. *Arctic Anthropology*, 45(2), 114-127.
152. Paul, D., Mandla, V. R., & Singh, T. (2017). Quantifying and modeling of stream network using digital elevation models. *Ain Shams Engineering Journal*, 8(3), 311-321.
153. Pelletier, C., Valero, S., Inglada, J., Champion, N., & Dedieu, G. (2016). Assessing the robustness of Random Forests to map land cover with high resolution satellite image time series over large areas. *Remote Sensing of Environment*, 187, 156-168.
154. Persendt, F. C., & Gomez, C. (2016). Assessment of drainage network extractions in a low-relief area of the Cuvelai Basin (Namibia) from multiple sources: LiDAR, topographic maps, and digital aerial orthophotographs. *Geomorphology*, 260, 32-50.
155. Pham, H. T., Marshall, L., Johnson, F., & Sharma, A. (2018). A method for combining SRTM DEM and ASTER GDEM2 to improve topography estimation in regions without reference data. *Remote Sensing of Environment*, 210, 229-241.
156. Pike, R. J., & Wilson, S. E. (1971). Elevation-relief ratio, hypsometric integral, and geomorphic area-altitude analysis. *Geological Society of America Bulletin*, 82(4), 1079-1084.

157. Pracilio, G., Smettem, K. R., Bennett, D., Harper, R. J., & Adams, M. L. (2006). Site assessment of a woody crop where a shallow hardpan soil layer constrained plant growth. *Plant and soil*, 288(1), 113-125.
158. Pramanik, S., & Punia, M. (2019). Land use/land cover change and surface urban heat island intensity: source–sink landscape-based study in Delhi, India. *Environment, Development and Sustainability*, 1-26.
159. Prasad, H. C., Bhalla, P., & Palria, S. (2014). Site suitability analysis of water harvesting structures using remote sensing and GIS-A case study of Pisangan watershed, Ajmer district, Rajasthan. *The International Archives of Photogrammetry, Remote Sensing and Spatial Information Sciences*, 40(8), 1471.
160. Qiu, F., Berglund, J., Jensen, J. R., Thakkar, P., & Ren, D. (2004). Speckle noise reduction in SAR imagery using a local adaptive median filter. *GIScience & Remote Sensing*, 41(3), 244-266.
161. Quinn, P. F. B. J., Beven, K., Chevallier, P., & Planchon, O. (1991). The prediction of hillslope flow paths for distributed hydrological modelling using digital terrain models. *Hydrological processes*, 5(1), 59-79.
162. Quiroga, V. M., Kurea, S., Udoa, K., & Manoa, A. (2016). Application of 2D numerical simulation for the analysis of the February 2014 Bolivian Amazonia flood: Application of the new HEC-RAS version 5. *Ribagua*, 3(1), 25-33.
163. Rakesh, K., Lohani, A. K., Sanjay, K., Chattered, C., & Nema, R. K. (2000). GIS based morphometric analysis of Ajay river basin upto Srarath gauging site of South Bihar. *Journal of Applied Hydrology*, 14(4), 45-54.
164. Ramli, N. A., Hamid, M. F. A., Azhan, N. H., & Ishak, M. A. A. S. (2019, July). Solar power generation prediction by using k-nearest neighbor method. In *AIP Conference Proceedings* (Vol. 2129, No. 1, p. 020116). AIP Publishing LLC.
165. Rana, V. K., & Suryanarayana, T. M. V. (2019). Visual and statistical comparison of ASTER, SRTM, and Cartosat digital elevation models for watershed. *Journal of Geovisualization and Spatial Analysis*, 3(2), 12.
166. Rana, V. K., & Suryanarayana, T. M. V. (2020). Performance evaluation of MLE, RF and SVM classification algorithms for watershed scale land use/land cover mapping using sentinel 2 bands. *Remote Sensing Applications: Society and Environment*, 19, 100351.
167. Ranagalage, M., Estoque, R. C., Zhang, X., & Murayama, Y. (2018). Spatial changes of urban heat island formation in the Colombo District, Sri Lanka: Implications for sustainability planning. *Sustainability*, 10(5), 1367.
168. Ranagalage, M., Murayama, Y., Dissanayake, D. M. S. L. B., & Simwanda, M. (2019). The impacts of landscape changes on annual mean land surface temperature in the tropical mountain city of Sri Lanka: A case study of Nuwara Eliya (1996–2017). *Sustainability*, 11(19), 5517.
169. Raouf, A., & Lichtenegger, J. (1997). Integrated use of SAR and optical data for coastal zone management. In *Third ERS Symposium on Space at the Service of Our Environment*, 414, 1089.
170. Rasul, A., Balzter, H., Ibrahim, G. R. F., Hameed, H. M., Wheeler, J., Adamu, B., ... & Najmaddin, P. M. (2018). Applying built-up and bare-soil indices from landsat 8 to cities in dry climates. *Land*, 7(3), 81.

171. Reddy, G. P. O., Maji, A. K., & Gajbhiye, K. S. (2004). Drainage morphometry and its influence on landform characteristics in a basaltic terrain, Central India—a remote sensing and GIS approach. *International Journal of Applied Earth Observation and Geoinformation*, 6(1), 1-16.
172. Rennó, C.D., Nobre, A.D., Cuartas, L.A., Soares, J.V., Hodnett, M.G., Tomasella, J., Waterloo, M.J., 2008. HAND, a new terrain descriptor using SRTM-DEM: mapping terra-firme rainforest environments in Amazonia. *Remote Sens. Environ.* 112 (9), 3469–3481.
173. Rincón, D., Khan, U. T., & Armenakis, C. (2018). Flood risk mapping using GIS and multi-criteria analysis: A greater Toronto area case study. *Geosciences*, 8(8), 275.
174. Rizeei, H. M., Pradhan, B., & Saharkhiz, M. A. (2018). Surface runoff prediction regarding LULC and climate dynamics using coupled LTM, optimized ARIMA, and GIS-based SCS-CN models in tropical region. *Arabian Journal of Geosciences*, 11(3), 53.
175. Rodriguez-Galiano, V. F., Ghimire, B., Rogan, J., Chica-Olmo, M., & Rigol-Sanchez, J. P. (2012). An assessment of the effectiveness of a random forest classifier for land-cover classification. *ISPRS Journal of Photogrammetry and Remote Sensing*, 67, 93-104.
176. Ross, C. W., Prihodko, L., Anchang, J., Kumar, S., Ji, W., & Hanan, N. P. (2018). HYSOGs250m, global gridded hydrologic soil groups for curve-number-based runoff modeling. *Scientific data*, 5(1), 1-9.
177. Rozos, D., Bathrellos, G. D., & Skillodimou, H. D. (2011). Comparison of the implementation of rock engineering system and analytic hierarchy process methods, upon landslide susceptibility mapping, using GIS: a case study from the Eastern Achaia County of Peloponnesus, Greece. *Environmental Earth Sciences*, 63(1), 49-63.
178. Rundquist, D. C., Narumalani, S., & Narayanan, R. M. (2001). A review of wetlands remote sensing and defining new considerations.
179. Saaty, T. L. (1977). A scaling method for priorities in hierarchical structures. *Journal of mathematical psychology*, 15(3), 234-281.
180. Saaty, T. L. (1987). Rank generation, preservation, and reversal in the analytic hierarchy decision process. *Decision sciences*, 18(2), 157-177.
181. Saaty, T. L. (1990). How to make a decision: the analytic hierarchy process. *European Journal of Operational Research*, 48(1), 9e26
182. Sarangi, A., Bhattacharya, A. K., Singh, A., & Singh, A. K. (2001). Use of Geographic Information System (GIS) in assessing the erosion status of watersheds. *Indian J Soil Conserv*, 29(19), F195.
183. Scanlon, B. R., Keese, K. E., Flint, A. L., Flint, L. E., Gaye, C. B., Edmunds, W. M., & Simmers, I. (2006). Global synthesis of groundwater recharge in semiarid and arid regions. *Hydrological Processes: An International Journal*, 20(15), 3335-3370.
184. Senthilnath, J., Shenoy, H. V., Rajendra, R., Omkar, S. N., Mani, V., & Diwakar, P. G. (2013). Integration of speckle de-noising and image segmentation using Synthetic Aperture Radar image for flood extent extraction. *Journal of earth system science*, 122(3), 559-572.
185. Serpico, S. B., Dellepiane, S., Boni, G., Moser, G., Angiati, E., & Rudari, R. (2012). Information extraction from remote sensing images for flood monitoring and damage evaluation. *Proceedings of the IEEE*, 100(10), 2946-2970.

186. Serpico, S. B., Dellepiane, S., Boni, G., Moser, G., Angiati, E., & Rudari, R. (2012). Information extraction from remote sensing images for flood monitoring and damage evaluation. *Proceedings of the IEEE*, 100(10), 2946-2970.
187. Shafizadeh-Moghadam, H., Weng, Q., Liu, H., & Valavi, R. (2020). Modeling the spatial variation of urban land surface temperature in relation to environmental and anthropogenic factors: a case study of Tehran, Iran. *GIScience & Remote Sensing*, 57(4), 483-496.
188. Shamsoddini, A., Trinder, J. C., Wagner, W., & Székely, B. (2010). *Image texture preservation in speckle noise suppression* (pp. 239-244). na.
189. Sharma, A., & Tiwari, K. N. (2014). A comparative appraisal of hydrological behavior of SRTM DEM at catchment level. *Journal of Hydrology*, 519, 1394-1404.
190. Sheng, Y., & Xia, Z. G. (1996, May). A comprehensive evaluation of filters for radar speckle suppression. In *IGARSS'96. 1996 International Geoscience and Remote Sensing Symposium* (Vol. 3, pp. 1559-1561). IEEE.
191. Shuai, T., Zhang, X., Wang, S., Zhang, L., Shang, K., Chen, X., & Wang, J. (2014). A spectral angle distance-weighting reconstruction method for filled pixels of the MODIS land surface temperature product. *IEEE Geoscience and Remote Sensing Letters*, 11(9), 1514-1518.
192. Singh, L. K., Jha, M. K., & Chowdary, V. M. (2017). Multi-criteria analysis and GIS modeling for identifying prospective water harvesting and artificial recharge sites for sustainable water supply. *Journal of Cleaner Production*, 142, 1436-1456.
193. Smith, K. G. (1950). Standards for grading texture of erosional topography. *American journal of Science*, 248(9), 655-668.
194. Sobrino, J. A., Jiménez-Muñoz, J. C., & Paolini, L. (2004). Land surface temperature retrieval from LANDSAT TM 5. *Remote Sensing of environment*, 90(4), 434-440.
195. Sørensen, R., & Seibert, J. (2007). Effects of DEM resolution on the calculation of topographical indices: TWI and its components. *Journal of Hydrology*, 347(1-2), 79-89.
196. Story, M., & Congalton, R. G. (1986). Accuracy assessment: a user's perspective. *Photogrammetric Engineering and remote sensing*, 52(3), 397-399.
197. Strahler, A. N. (1957). Quantitative analysis of watershed geomorphology. *Eos, Transactions American Geophysical Union*, 38(6), 913-920.
198. Strahler, A. N. (1964). Part II. Quantitative geomorphology of drainage basins and channel networks. *Handbook of Applied Hydrology: McGraw-Hill, New York*, 4-39.
199. Subedi, M., & Tamrakar, N. K. (2020). Fluvial Geomorphology and Basin Development of Karra Khola Basin, Hetauda, Central Nepal. *Journal of Geological Research*, 2(4).
200. Subramanya, K. (2013). *Engineering hydrology, 4e*. Tata McGraw-Hill Education.
201. Sudhakar, B. S., Anupam, K. S., & Akshay, O. J. (2015). Snyder unit hydrograph and GIS for estimation of flood for un-gauged catchments in lower Tapi basin, India. *Hydrology: Current Research*, 6(1), 1.
202. Sukristiyanti, S., Maria, R., & Lestiana, H. (2018, February). Watershed-based morphometric analysis: a review. In *IOP conference series: earth and environmental science* (Vol. 118, pp. 12-28). IOP Publishing.
203. Tağıl, Ş., & Jenness, J. (2008). GIS-based automated landform classification and topographic, landcover and geologic attributes of landforms around the Yazoren Polje, Turkey.

204. Tan, M. L., Ficklin, D. L., Dixon, B., Yusop, Z., & Chaplot, V. (2015). Impacts of DEM resolution, source, and resampling technique on SWAT-simulated streamflow. *Applied Geography*, *63*, 357-368.
205. Thakur, B., Parajuli, R., Kalra, A., Ahmad, S., & Gupta, R. (2017). Coupling HEC-RAS and HEC-HMS in precipitation runoff modelling and evaluating flood plain inundation map. In *World Environmental and Water Resources Congress 2017* (pp. 240-251).
206. Tomlinson, C. J., Chapman, L., Thornes, J. E., & Baker, C. (2011). Remote sensing land surface temperature for meteorology and climatology: A review. *Meteorological Applications*, *18*(3), 296-306.
207. Tripathi, S. S. (2018). Impact of land use land cover change on runoff using RS & GIS and curve number. *International Journal of Basic and Applied Agricultural Research*, *16*(3), 224-227.
208. Turner, B. L., Lambin, E. F., & Reenberg, A. (2007). The emergence of land change science for global environmental change and sustainability. *Proceedings of the National Academy of Sciences*, *104*(52), 20666-20671.
209. Vapnik, V. (2013). *The nature of statistical learning theory*. Springer science & business media.
210. Vozinaki, A. E. K., Morianou, G. G., Alexakis, D. D., & Tsanis, I. K. (2017). Comparing 1D and combined 1D/2D hydraulic simulations using high-resolution topographic data: A case study of the Koiliaris basin, Greece. *Hydrological Sciences Journal*, *62*(4), 642-656.
211. Wakode, H. B., Dutta, D., Desai, V. R., Baier, K., & Azzam, R. (2013). Morphometric analysis of the upper catchment of Kosi River using GIS techniques. *Arabian Journal of Geosciences*, *6*(2), 395-408.
212. Wang, W., Yang, X., & Yao, T. (2012). Evaluation of ASTER GDEM and SRTM and their suitability in hydraulic modelling of a glacial lake outburst flood in southeast Tibet. *Hydrological Processes*, *26*(2), 213-225.
213. Wang, X., Ge, L., & Li, X. (2012). Evaluation of filters for ENVISAT ASAR speckle suppression in pasture area. *ISPRS Annals of Photogrammetry, Remote Sensing and Spatial Information Sciences*, *7*, 341-346.
214. Weerasinghe, H., Schneider, U. A., & Loew, A. (2011). Water harvest-and storage-location assessment model using GIS and remote sensing. *Hydrology and Earth System Sciences Discussions*, *8*(2), 3353-3381.
215. Weiss, A. (2001, July). Topographic position and landforms analysis. In *Poster presentation, ESRI user conference, San Diego, CA* (Vol. 200).
216. Wendler, T., & Gröttrup, S. (2016). *Data mining with SPSS modeler: theory, exercises and solutions*. Springer.
217. Weng, Q. (2001). A remote sensing? GIS evaluation of urban expansion and its impact on surface temperature in the Zhujiang Delta, China. *International journal of remote sensing*, *22*(10), 1999-2014.
218. Weng, Q. (Ed.). (2007). *Taylor & Francis Series in Remote Sensing Applications*. CRC Press, Taylor & Francis Group.
219. Weng, Q., Lu, D., & Schubring, J. (2004). Estimation of land surface temperature–vegetation abundance relationship for urban heat island studies. *Remote sensing of Environment*, *89*(4), 467-483.

220. Wilson, J. P., & Gallant, J. C. (Eds.). (2000). *Terrain analysis: principles and applications*. John Wiley & Sons.
221. Winter, T. C., & LaBaugh, J. W. (2003). Hydrologic considerations in defining isolated wetlands. *Wetlands*, 23(3), 532-540.
222. Wolock, D. M., & Price, C. V. (1994). Effects of digital elevation model map scale and data resolution on a topography-based watershed model. *Water Resources Research*, 30(11), 3041-3052.
223. Wu, R. S., Molina, G. L. L., & Hussain, F. (2018). Optimal sites identification for rainwater harvesting in northeastern Guatemala by analytical hierarchy process. *Water resources management*, 32(12), 4139-4153.
224. Wu, T., & Han, L. (2019). Cloud Extraction Scheme for Multi-Spectral Images Using Landsat-8 OLI Images With High Brightness Reflectivity Covered. *IEEE Access*, 8, 3387-3396.
225. Xu, S. (2009). An approach to analyzing the intensity of the daytime surface urban heat island effect at a local scale. *Environmental monitoring and assessment*, 151(1-4), 289.
226. Yang, C., Everitt, J. H., & Murden, D. (2011). Evaluating high resolution SPOT 5 satellite imagery for crop identification. *Computers and Electronics in Agriculture*, 75(2), 347–354. <https://doi.org/10.1016/j.compag.2010.12.012>
227. Yu, L., Liang, L., Wang, J., Zhao, Y., Cheng, Q., Hu, L., ... & Gong, P. (2014). Meta-discoveries from a synthesis of satellite-based land-cover mapping research. *International Journal of Remote Sensing*, 35(13), 4573-4588.
228. Zakerinejad, R. (2016). *Integrated Assessment of Gully Erosion Processes, Using Multispectral Remote Sensing, Stochastic Modelling, and GIS-based Morphotectonic Analysis; A Case Study in the Southwest of Iran* (Doctoral dissertation, Universitätsbibliothek Tübingen).
229. Zeng, C., Shen, H., Zhong, M., Zhang, L., & Wu, P. (2014). Reconstructing MODIS LST based on multitemporal classification and robust regression. *IEEE Geoscience and Remote Sensing Letters*, 12(3), 512-516.
230. Zhang, F., Zhu, X., & Liu, D. (2014). Blending MODIS and Landsat images for urban flood mapping. *International journal of remote sensing*, 35(9), 3237-3253.
231. Zhang, S. Q., Zhang, S. K., & Zhang, J. Y. (2000). A study on wetland classification model of remote sensing in the Sangjiang Plain. *Chinese Geographical Science*, 10(1), 68-73.
232. Zhang, X., Estoque, R. C., & Murayama, Y. (2017). An urban heat island study in Nanchang City, China based on land surface temperature and social-ecological variables. *Sustainable cities and society*, 32, 557-568.
233. Zhao, M., Cai, H., Qiao, Z., & Xu, X. (2016). Influence of urban expansion on the urban heat island effect in Shanghai. *International Journal of Geographical Information Science*, 30(12), 2421-2441.
234. Zölch, T., Maderspacher, J., Wamsler, C., & Pauleit, S. (2016). Using green infrastructure for urban climate-proofing: An evaluation of heat mitigation measures at the micro-scale. *Urban Forestry & Urban Greening*, 20, 305-316.